Many Body Linear Kicked Rotor

A Thesis

submitted to
Indian Institute of Science Education and Research Pune
in partial fulfillment of the requirements for the
BS-MS Dual Degree Programme

by

Anjali Nambudiripad

Indian Institute of Science Education and Research Pune
Dr. Homi Bhabha Road,
Pashan, Pune 411008, INDIA.

January, 2021

Supervisor: Dr. M. S. Santhanam

Certificate

This is to certify that this dissertation entitled Many Body Linear Kicked Rotor towards the partial fulfilment of the BS-MS dual degree programme at the Indian Institute of Science Education and Research, Pune represents study/work carried out by Anjali Nambudiripad at Indian Institute of Science Education and Research under the supervision of Dr. M. S. Santhanam, Professor, Department of Physics , during the academic year 2020-2021.

24.12.2020

Dr. M. S. Santhanam

Committee:

Dr. M. S. Santhanam

Dr. Rejish Nath

To my family, who always stood by me and encouraged me to follow my dreams.

Declaration

I hereby declare that the matter embodied in the report entitled Many Body Linear Kicked Rotor are the results of the work carried out by me at the Department of Physics, Indian Institute of Science Education and Research, Pune, under the supervision of Dr. M. S. Santhanam and the same has not been submitted elsewhere for any other degree.

Anjali Nambudiripad

Acknowledgments

I would like to thank, first and foremost, my supervisor Dr. M. S. Santhanam, whose guidance and support has been invaluable throughout this project.

I would also like to show my appreciation to the TAC member for my thesis, Dr. Rejish Nath, for his input on my project.

Lastly, I must express my profound gratitude to my family and friends who have always supported me and encouraged me through my toughest times, especially my parents and brother without whose unwavering belief in me, I wouldn't be where I am today.

Abstract

In this thesis, we have calculated the bipartite entanglement entropy of the quantum many-body linear kicked rotor system. We have looked at how this entropy changes with time and with the parameter of the system. The classical version of this system is unique in that it shows no chaotic dynamics for any value of kicking strength. We have tried to induce chaos into this system by introducing a momentum interaction term. This changes the quantum dynamics of the system and its spectral statistics.

Contents

Introduction

Quantum kicked rotor has been used as a simple model to study Hamiltonian chaos. In more recent times, there has been greater interest in the many body versions of this model to study the phenomenon of many body localisation. Many body localisation is a distinctly quantum phenomenon in which all the eigenvalues of the system are localised instead of achieving thermal equilibrium. It's a relatively new field of study that makes us revisit the fundamentals of quantum statistical mechanics.

The many-body localised linear kicked rotor is unique in that it is a fully integrable system that shows exact correspondence in dynamics between the quantum and classical versions. The many-body localisation in the system is also parameter dependent. So based on different values of these parameters, the system can show both localised as well as delocalised dynamics. We wanted to look at how these changes in the dynamics, localisation or delocalisation, affect the correlation (entanglement) between the particles in the system. To quantify this entanglement, we have endeavoured to calculate the entanglement entropy for the system.

Since neither the classical nor the quantum versions of the system show any signs of chaos, we looked at inducing chaos into the classical system and quantifying the chaos in various ways. We did this by introducing a momentum interaction term in place of interaction in the position term. Once we had chaos in the classical system, we looked at how this affected the quantum regime for this system, if we see chaos in the quantum system or if the system still shows localisation and delocalisation.

Chapter 1

The Model

Keser, Ganeshan, Refael and Galitski in their paper give the generalised model of an interacting linear kicked rotor that is exactly solvable. The Hamiltonian for this system is given by,

$$\hat{H} = \hat{H}_0 + \hat{V} \sum_{n=-\infty}^{\infty} \delta(t-n), \qquad with \qquad \hat{V} = \sum_{i}^{d} K_i(\hat{\theta}_i) \tag{1.1}$$

$$\hat{H_0} = 2\pi \sum_{i=1}^{d} \alpha_i \hat{p}_i + \frac{1}{2} \sum_{i \neq j}^{d-1} J_{ij}(\hat{\theta}_i - \hat{\theta}_j). \tag{1.2}$$

Here, $\hat{H}_0$ is the static Hamiltonian that is linearly dependent on the momentum operator and contains an interaction term. It describes d interacting particles on a ring moving at a constant speed of $2\pi\alpha_i$ radians per one period of kick. J_{ij} is the interacting two-body potential that is translationally invariant. This results in conservation of momentum for the system. The kicking potential is given by $\hat{V}$ which contains the delta function impulses, the periodic kicks and the kicking strength given by a generic periodic function $K_i(\hat{\theta}_i)$. This $K_i(\hat{\theta}_i)$ is periodic in 2π and they have taken its Fourier expansion to give, $K_i(\hat{\theta}_i) = \sum_m k_m e^{im\theta_i}$, where k_m are the arbitrary Fourier coefficients. Similarly J_{ij} has been expanded to give $J_{ij}(\hat{\theta}_i - \hat{\theta}_j) = \sum_m b_m^{ij} e^{im(\theta_i - \theta_j)}$. Here, b_m^{ij} are the Fourier coefficients of the interacting potential between the i-th and the j-th particles.

The main aim of their paper is to show that dynamical many body localisation in the momentum basis exists for this system and it is shown using three quantifiers namely energy

growth over long times, momentum degrees of freedom over long times and the existence of integrals of motion.

They had obtained analytical expressions for these three quantities which are:

1. **Average energy after N kicks**, $E(N) = \langle\Psi_N| \hat{H}_0 |\Psi_N\rangle$

$$E(N) = E(0) + \sum_{i=1}^{d} \sum_{m} 2\pi\alpha_i \langle\hat{\Gamma}_{mi}\rangle_0 \frac{\sin(mN\pi\alpha_i)}{\sin(m\pi\alpha_i)} \tag{1.3}$$

   $|\Psi_N\rangle = \hat{U}_F^N |\Psi_0\rangle$, $\hat{U}_F = e^{-i\hat{V}} e^{-i\hat{H}_0}$ where $\hat{U}_F$ is the Floquet evolution operator. $E(0) = \langle\Psi_0| \hat{H}_0 |\Psi_0\rangle$ is the average energy over the initial state. $\hat{\Gamma}_{mi} = -imk_m e^{im(\hat{\theta}_i + \pi\alpha_i[N+1])}$ depends on the form of $K_i(\hat{\theta}_i)$ chosen. Since $\hat{\Gamma}_{mi}$ is a bounded function of number of kicks N, energy growth is dependent on the ratio $\frac{\sin(mN\pi\alpha_i)}{\sin(m\pi\alpha_i)}$. If the denominator blows up, the total energy average will become delocalised. In the derivation of this result, they have shown that the translational invariance of the interaction potential ensures conservation of momentum during interactions and that, coupled with the linear dependence of the Hamiltonian of the system on the momentum, leads to the total energy becoming independent of an interaction term. This no longer holds if the interaction potential is not translationally invariant.

2. **Spread in momentum degrees of freedom over long time**, $\hat{p}_i(N) = \langle\Psi_N| \hat{p}_i |\Psi_N\rangle$

$$p_i(N) = \langle\hat{p}_i\rangle_0 + \sum_{m} \langle\hat{\Gamma}_{mi}\rangle_0 \frac{\sin(mN\pi\alpha_i)}{\sin(m\pi\alpha_i)} + \sum_{mj} \langle\hat{\Gamma}^{int}_{mij}\rangle_0 \frac{\sin(mN\pi\Delta\alpha_{ij})}{m\pi\Delta\alpha_{ij}} \tag{1.4}$$

   Here, $\Delta\alpha_{ij} = \alpha_i - \alpha_j$. The first term $\langle\hat{p}_i\rangle_0$ is the momentum of the ith particle averaged over the initial wave-function. The second term corresponds to the kicking potential and is the same as defined for the energy growth. The third term corresponds to the interaction potential. $\Gamma^{int}_{mij} = -imb^{ij}_m e^{im(\hat{\theta}_i - \hat{\theta}_j + \pi N\Delta\alpha_{ij})}$ and is again a bounded function of N. Therefore, the growth of the momenta come from the ratio, $\frac{\sin(mN\pi\Delta\alpha_{ij})}{m\pi\Delta\alpha_{ij}}$. If the denominator diverges, the momentum growth will be delocalised.

3. **Existence of integrals of motion in the momentum basis**

   To construct the integrals of motion, they identify d operators $\hat{C}_i$ such that $[\hat{C}_i, \hat{U}_F] = 0$ and $[\hat{C}_i, \hat{C}_j] = 0$. These operators then satisfy the property that $\langle\hat{C}_i\rangle_{N+1} = \langle\hat{C}_i\rangle_N$ and

are given by,

$$\hat{C}_i = \hat{p}_i + \frac{1}{2}\sum_m \frac{m k_m e^{im(\hat{\theta}_i + \pi\alpha_i)}}{\sin(m\pi\alpha_i)} + \frac{1}{2}\sum_{mj} \frac{b_m^{ij} e^{im(\hat{\theta}_i - \hat{\theta}_j)}}{\pi\Delta\alpha_{ij}} \tag{1.5}$$

Here, since the $\hat{C}_i$ are integrals of motion, the $\hat{p}_i$ will be bounded as long as the other two terms converge. Therefore the existence of these integrals of motion depend on θ dependant terms in the equation and whether their denominators diverge or not.

For the system at hand, there always exist d integrals of motion corresponding to the spatial variables, $\hat{B}_i = \hat{\theta}_i/\alpha_i \, (mod\, 2\pi)$, $[\hat{B}_i, \hat{U}_F] = 0$. These integrals of motion however do not contribute to the many body localisation in the system since they do not have momentum dependence. These $\hat{B}_i$ therefore ensure integrability of the model even if the $\hat{C}_i$ do not exist.

Keser et. al. then give the three cases of α_i for which localisation or delocalisation is observed.

- **Case 1: All the α_i are distinct irrationals**

  In this case, all the denominators in the three quantities exist. The energy growth as well as momentum growth are bounded for large N. All d of the integrals of motion $\hat{C}_i$ also exist. There is complete many body localisation in this case.

- **Case 2: $\alpha_1 = \frac{1}{2}$ and $\alpha_2 ... \alpha_d$ are distinct irrationals**

  In this case, the $\sin(m\pi\alpha_i)$ in the denominators of the kicking potential terms of the three quantities go to zero for $m = 2$ and these denominators blow up. This happens for any of the α_i if they are rationals since there will be an m such that $m\alpha_i$ is an integer making these terms diverge. Thus for this case, the momentum corresponding to particle 1 as well as the energy blow up and the $\hat{C}_1$ corresponding to α_1 does not exist even though the other $\hat{C}_i$ do exist. Therefore in this case there is delocalisation in energy as well as $\hat{p}_1$ but localisation for all the other momenta and this is reflected in the integrals of motion.

- **Case 3: $\alpha_1 = \alpha_2$ and $\alpha_2 ... \alpha_d$ are distinct irrationals**

  In this case, the interaction terms in the momenta and integrals of motion for particles 1 and 2 diverge due to their denominator $(\alpha_1 - \alpha_2)$ going to 0. Total energy however stays bounded since it does not depend on interaction. This is due to the translational

invariance of the interaction potential which results in conservation of momentum. Physically what this means is that for each pair of particles, each interaction results in the exchange of momentum. This results in the total momentum and energy being unaffected by the interactions. The momenta for particles other than 1 and 2 are also bounded and the integrals of motion corresponding to them also exist. Thus there is localisation of the total energy as well as momenta for particles 3 to d and delocalisation of the momenta for particles 1 and 2. This is evidenced in the existence of $\hat{C}_i$ as they do not exist for particles 1 and 2 and do exist for the rest. This case is special in that it only exists for this model due to the translational invariance of the interaction potential. If this property is broken, this will no longer hold.

1.1 Re-creation of the results of the paper

We attempted to re-create the results of the paper, mainly, the localisation and delocalisation observed in energy and momenta plots for various values of α_i. We did this for a simplified version of their model given in equations (1.1) and (1.2).

For our simplified system, the unperturbed Hamiltonian is given by,

$$\hat{H}_0 = 2\pi\alpha_1\hat{p}_1 + 2\pi\alpha_2\hat{p}_2 + \cos\Big(\hat{\theta}_1 - \hat{\theta}_2\Big) \tag{1.6}$$

And the kicking potential is given by,

$$\hat{V} = \cos\Big(\hat{\theta}_1\Big) + \cos\Big(\hat{\theta}_2\Big) \tag{1.7}$$

The hamiltonian of the system is then,

$$\hat{H} = 2\pi\alpha_1\hat{p}_1 + 2\pi\alpha_2\hat{p}_2 + \cos\Big(\hat{\theta}_1 - \hat{\theta}_2\Big) + \left[\cos\Big(\hat{\theta}_1\Big) + \cos\Big(\hat{\theta}_2\Big)\right] \sum_{n=-\infty}^{\infty} \delta(t-n) \tag{1.8}$$

Therefore we are looking at a 2-particle system with simple cosine potentials. This simplification of the potentials causes a minor difference to the values of α_i that correspond to the three cases that Keser et. al. enumerated.

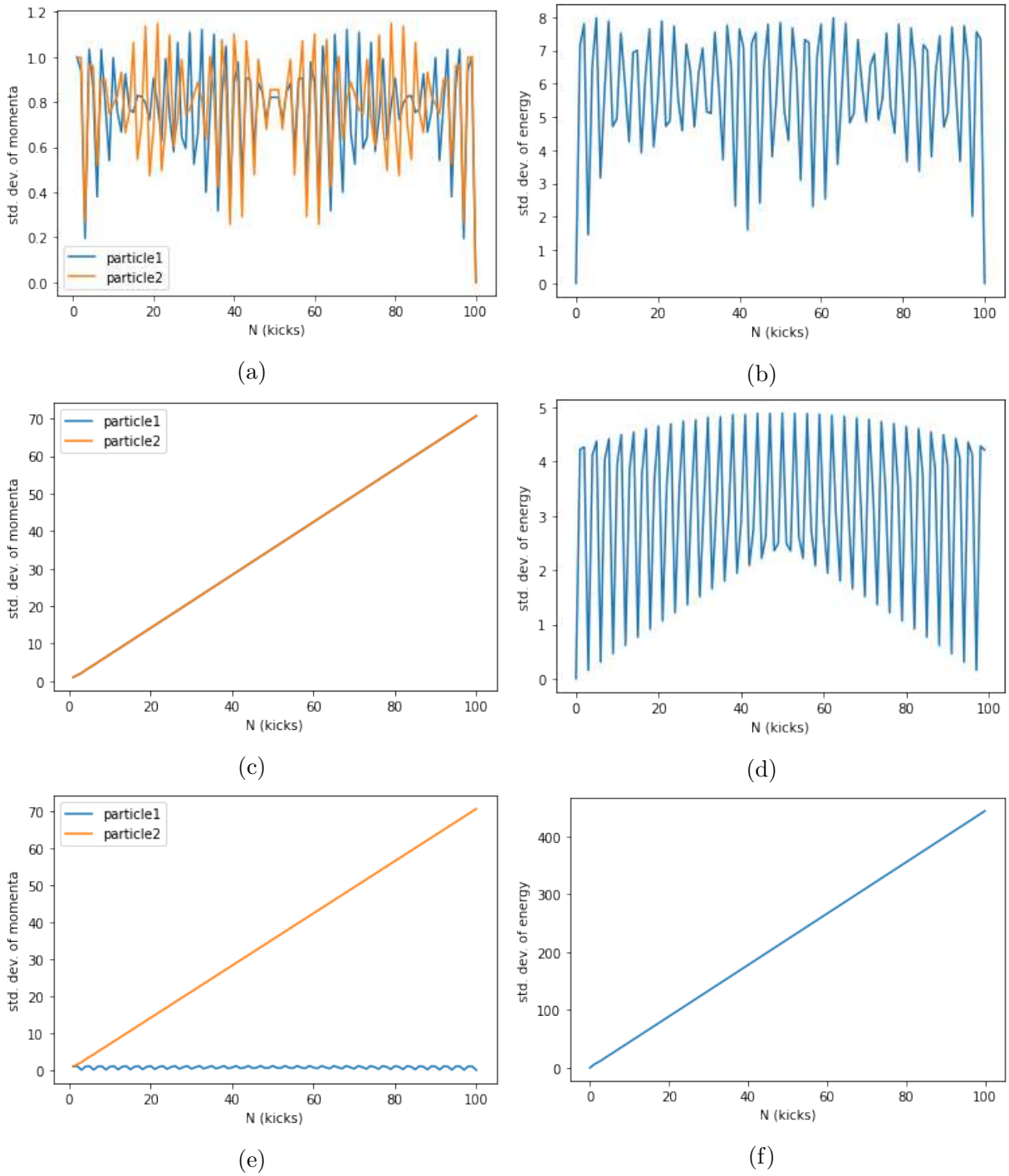

Figure 1.1: Momentum and energy standard deviation plots to show the evolution of these quantities for the simplified system. Momentum and energy evolution respectively for (a),(b) $\alpha_1 = 0.67$ and $\alpha_2 = 1.31$ (Case 1); (c),(d) $\alpha_1 = 0.67$ and $\alpha_2 = 0.67$ (Case 3); (e),(f) $\alpha_1 = 0.67$ and $\alpha_2 = 1$ (Case 2).

- Case 1:

  This case now holds if both the α_i are simply distinct and non-integers. This is because the denominator of the kicking term in the equations (1.3), (1.4) and (1.5) are now $\sin(\pi\alpha_i)$. So as long as α_i is not an integer, these equations will be localised.

- Case 2:

  This case holds if α_1 is an integer while α_2 is a non-integer. This is for the same reasons given in case 1.

- Case 3:

  This case holds if $\alpha_1 = \alpha_2$. This case is the same as for the case in the model given by Keser et. al.

We have plotted the momentum and energy standard deviations in Fig.(1.1), which show the evolution of these quantities. We see the localisation as well as delocalisation for the three cases of α_i, as mentioned above.

Chapter 2

Entropy Calculation for the Quantum Linear Kicked Rotor System

Entanglement entropy is a way to quantify entanglement present in any given system. We calculate the entanglement entropy for the evolution wave-function as well as for the quasi-energy wave-function of the quantum linear kicked rotor system and look at how it changes with different localisation and delocalisation of the dynamics of the system. We have also calculated the information entropy which quantifies the amount of information stored in any given system.

2.1 Entanglement Entropy for a Continuous Variable System

The system we are working with is a continuous variable system where the wave-functions are in the position basis representation. Therefore to calculate the entanglement entropy for such a system we need to calculate the density operator as well as its reduced density operators in the continuous position basis.

The density operator of a system is defined as,

$$\rho = |\Psi\rangle \langle\Psi| \tag{2.1}$$

For two particles, this wave-function can be written as,

$$|\psi\rangle = \int d\theta_1\, d\theta_2 \Psi(\theta_1, \theta_2)\, |\theta_1\rangle\, |\theta_2\rangle \tag{2.2}$$

This gives the density matrix as,

$$\rho = \int d\theta_1\, d\theta_2\, d\theta_1^{'}\, d\theta_2^{'} \Psi(\theta_1, \theta_2)\Psi^*(\theta_1^{'}, \theta_2^{'})\, |\theta_1\rangle\, \langle\theta_1^{'}|\, |\theta_2\rangle\, \langle\theta_2^{'}| \tag{2.3}$$

Here the kernel of the density operator is given by,

$$\rho = \Psi(\theta_1, \theta_2)\Psi^*(\theta_1^{'}, \theta_2^{'}) \tag{2.4}$$

To calculate the partial trace for this density operator we proceed as follows:

Taking partial trace over the outer product of the position basis states,

$$\mathrm{tr}_2(\, |\theta_1\rangle\, \langle\theta_1^{'}|\, |\theta_2\rangle\, \langle\theta_2^{'}|\,) = |\theta_1\rangle\, \langle\theta_1^{'}|\, \mathrm{tr}_2(\, |\theta_2\rangle\, \langle\theta_2^{'}|\,) \tag{2.5}$$

Therefore,

$$\mathrm{tr}_2(\, |\theta_1\rangle\, \langle\theta_1^{'}|\, |\theta_2\rangle\, \langle\theta_2^{'}|\,) = |\theta_1\rangle\, \langle\theta_1^{'}|\, \delta(\theta_2 - \theta_2^{'}) \tag{2.6}$$

This gives the reduced density operator for the first particle as,

$$\rho_1 = \int d\theta_1\, d\theta_2\, d\theta_1^{'} \Psi(\theta_1, \theta_2)\Psi^*(\theta_1^{'}, \theta_2)\, |\theta_1\rangle\, \langle\theta_1^{'}| \tag{2.7}$$

Similarly, the reduced density matrix for the second particle can be written as,

$$\rho_2 = \int d\theta_1\, d\theta_2\, d\theta_2^{'} \Psi(\theta_1, \theta_2)\Psi^*(\theta_1, \theta_2^{'})\, |\theta_2\rangle\, \langle\theta_2^{'}| \tag{2.8}$$

For the first particle, the reduced density matrix kernel is,

$$\rho_1(\theta_1, \theta_1^{'}) = \langle\theta_1|\, \rho_1\, |\theta_1^{'}\rangle = \int d\theta_2 \Psi(\theta_1, \theta_2)\Psi^*(\theta_1^{'}, \theta_2) \tag{2.9}$$

For continuous variable systems, the eigenvalue equation for this reduced density matrix can be written as,

$$\int d\theta_1^{'} \rho_1(\theta_1, \theta_1^{'})\phi_i(\theta_1^{'}) = \lambda_i \phi_i(\theta_1) \tag{2.10}$$

Where λ_i is the ith eigenvalue and ϕ_i is the ith eigenfunction.

To solve for these eigenvalues of the reduced density matrix, we proceed by discretizing the above equation,

$$\delta \sum_{p=0}^{n} \rho_{pq}\phi_p = \lambda_q \phi_q \tag{2.11}$$

Where, $\delta = 2\pi/n$, with n divisions between $0 < \theta_1 \leq 2\pi$ and $0 < \theta_1^{'} \leq 2\pi$, such that $n \to \infty$. This gives a discretised ρ_1 in matrix form for which we can solve its characteristic equation to find the eigenvalues.

Now, we proceed, using the procedure described above, to calculate the reduced density matrices for the wave-functions of the simplified model system whose Hamiltonian is given by equation (1.8) as well as the 3-particle version of the same system.

2.1.1 Calculating entanglement entropy for the evolution wave-function (2-particles)

For the 2-particle system with the Hamiltonian given in equation (1.8), the evolution wave-function is given by,

$$\Psi_N(\theta_1, \theta_2) = e^{-i\sum_{n=1}^{N}[\cos(\theta_1+2\pi n\alpha_1)+\cos(\theta_2+2\pi n\alpha_2)+\cos(\theta_1-\theta_2+2\pi n(\alpha_1-\alpha_2))]}\psi_0(\theta_1, \theta_2), \tag{2.12}$$

where ψ_0 is the initial wave-function and we have chosen it to be,

$$\psi_0(\theta_1, \theta_2) = \frac{1}{2\pi} e^{i(p_0^1\theta_1 + p_0^2\theta_2)} \tag{2.13}$$

For this wave-function, the reduced density matrix kernel is, from (2.9),

$$\begin{aligned}\rho_1(\theta_1, \theta_1^{'}) = \int_0^{2\pi} d\theta_2 \frac{1}{(2\pi)^2} e^{ip_0^1(\theta_1-\theta_1^{'})} e^{-i\sum_{n=1}^{N}\left[\cos(\theta_1+2\pi n\alpha_1)-\cos\left(\theta_1^{'}+2\pi n\alpha_1\right)\right]} \\ \times e^{-i\sum_{n=1}^{N}\left[\cos(\theta_1-\theta_2+2\pi n(\alpha_1-\alpha_2))-\cos\left(\theta_1^{'}-\theta_2+2\pi n(\alpha_1-\alpha_2)\right)\right]}\end{aligned} \tag{2.14}$$

We can simplify the summations using the identity,

$$\sum_{n=1}^{N} \cos(\theta_1 + 2\pi n\alpha_1) = \frac{\sin(N\pi\alpha_1)}{\sin(\pi\alpha_1)} \cos(\theta_1 + (N+1)\pi\alpha_1) \tag{2.15}$$

Then,

$$\begin{aligned}\rho_1(\theta_1, \theta_1^{'}) = \int_0^{2\pi} d\theta_2 \frac{1}{(2\pi)^2} e^{ip_0^1(\theta_1 - \theta_1^{'})} e^{-i\frac{\sin(N\pi\alpha_1)}{\sin(\pi\alpha_1)}\left[\cos(\theta_1+(N+1)\pi\alpha_1) - \cos\left(\theta_1^{'}+(N+1)\pi\alpha_1\right)\right]} \\ \times e^{-i\frac{\sin(N\pi(\alpha_1-\alpha_2))}{\sin(\pi(\alpha_1-\alpha_2))}\left[\cos(\theta_1-\theta_2+(N+1)\pi(\alpha_1-\alpha_2)) - \cos\left(\theta_1^{'}-\theta_2+(N+1)\pi(\alpha_1-\alpha_2)\right)\right]}\end{aligned} \tag{2.16}$$

Using trigonometric identities, we have,

$$\begin{aligned}&\cos(\theta_1 - \theta_2 + (N+1)\pi(\alpha_1 - \alpha_2)) - \cos\left(\theta_1^{'} - \theta_2 + (N+1)\pi(\alpha_1 - \alpha_2)\right) \\ &\quad = 2\sin\left(\frac{\theta_1 + \theta_1^{'}}{2} - \theta_2 + (N+1)\pi(\alpha_1 - \alpha_2)\right) \sin\left(\frac{\theta_1^{'} - \theta_1}{2}\right)\end{aligned} \tag{2.17}$$

Plugging this into (2.16) we get,

$$\begin{aligned}\rho_1(\theta_1, \theta_1^{'}) = \int_0^{2\pi} d\theta_2 \frac{1}{(2\pi)^2} e^{ip_0^1(\theta_1 - \theta_1^{'})} e^{-i\frac{\sin(N\pi\alpha_1)}{\sin(\pi\alpha_1)}\left[\cos(\theta_1+(N+1)\pi\alpha_1) - \cos\left(\theta_1^{'}+(N+1)\pi\alpha_1\right)\right]} \\ \times \quad e^{-2i\frac{\sin(N\pi(\alpha_1-\alpha_2))}{\sin(\pi(\alpha_1-\alpha_2))}\sin\left(\frac{\theta_1+\theta_1^{'}}{2} - \theta_2 + (N+1)\pi(\alpha_1-\alpha_2)\right)\sin\left(\frac{\theta_1^{'}-\theta_1}{2}\right)}\end{aligned} \tag{2.18}$$

This can be represented in simple form as,

$$\begin{aligned}\rho_1(\theta_1, \theta_1^{'}) &= \int_0^{2\pi} \frac{d\theta_2}{2\pi} C_1 e^{iC_2\sin(\theta_2 + C_3)} \\ &= \int_0^{2\pi} \frac{d\theta_2}{2\pi} C_1 e^{iC_2\sin(\theta_2)} \\ &= C_1 J_0(C_2)\end{aligned} \tag{2.19}$$

Where $J_0(C_2)$ is the bessel function of the first kind and C_1 and C_2 are constants with respect to the integration such that,

$$C_1 = \frac{1}{2\pi} e^{ip_0^1(\theta_1 - \theta_1^{'})} e^{-i\frac{\sin(N\pi\alpha_1)}{\sin(\pi\alpha_1)}\left[\cos(\theta_1+(N+1)\pi\alpha_1) - \cos\left(\theta_1^{'}+(N+1)\pi\alpha_1\right)\right]} \tag{2.20}$$

$$C_2 = 2\frac{\sin(N\pi(\alpha_1 - \alpha_2))}{\sin(\pi(\alpha_1 - \alpha_2))}\sin\left(\frac{\theta_1^{'} - \theta_1}{2}\right) \tag{2.21}$$

Equation (2.19) then gives the reduced density matrix for the first particle which we can discretise in θ_1 and $\theta_1^{'}$ variables to find the eigenvalues λ_i of the matrix as in equation (2.11).

The bipartite entanglement entropy for this reduced state is then,

$$S = -\sum_i \left(\frac{\lambda_i}{\sum_s \lambda_s}\log_2\left(\frac{\lambda_i}{\sum_t \lambda_t}\right)\right) \tag{2.22}$$

Here the $\sum_s \lambda_s$ in the denominator is used to normalise the eigenvalues.

2.1.2 Calculating the entanglement entropy for the evolution wave-function (3-particles)

We extend the simplified model from equation (1.8) from 2 to 3 particles. The Hamiltonian of the system then is,

$$\begin{aligned}\hat{H} = 2\pi\alpha_1\hat{p}_1 + 2\pi\alpha_2\hat{p}_2 + 2\pi\alpha_3\hat{p}_3 + \cos\left(\hat{\theta}_1 - \hat{\theta}_2\right) + \cos\left(\hat{\theta}_1 - \hat{\theta}_3\right) + \cos\left(\hat{\theta}_2 - \hat{\theta}_3\right) \\ + \left[\cos\left(\hat{\theta}_1\right) + \cos\left(\hat{\theta}_2\right) + \cos\left(\hat{\theta}_3\right)\right]\sum_{n=-\infty}^{\infty}\delta(t-n)\end{aligned} \tag{2.23}$$

The evolution wave-function for this Hamiltonian is given by,

$$\Psi_N(\theta_1, \theta_2, \theta_3) = e^{-i\sum_{n=1}^{N}[\sum_{j=1}^{3}\cos(\theta_j + 2\pi n\alpha_j) + \frac{1}{2}\sum_{j\neq k}^{3}\cos(\theta_j - \theta_k + 2\pi n(\alpha_j - \alpha_k))]}\psi_0(\theta_1, \theta_2, \theta_3) \tag{2.24}$$

Where ψ_0 is the initial wave-function and is chosen to be,

$$\psi_0(\theta_1, \theta_2, \theta_3) = \frac{1}{(2\pi)^{(3/2)}}e^{i(p_0^1\theta_1 + p_0^2\theta_2 + p_0^3\theta_3)} \tag{2.25}$$

Using the trigonometric identities as in (2.15) and (2.17), we can write the reduced density matrix of the first particle for this wave-function as,

$$\begin{aligned}\rho_1(\theta_1,\theta_1^{'}) = \frac{1}{(2\pi)^3}e^{ip_0^1(\theta_1-\theta_1^{'})}e^{-i\frac{\sin(N\pi\alpha_1)}{\sin(\pi\alpha_1)}\left[\cos(\theta_1+(N+1)\pi\alpha_1)-\cos\left(\theta_1^{'}+(N+1)\pi\alpha_1\right)\right]} \\ \times\int_0^{2\pi}d\theta_2 e^{-2i\frac{\sin(N\pi(\alpha_1-\alpha_2))}{\sin(\pi(\alpha_1-\alpha_2))}\sin\left(\frac{\theta_1+\theta_1^{'}}{2}-\theta_2+(N+1)\pi(\alpha_1-\alpha_2)\right)\sin\left(\frac{\theta_1^{'}-\theta_1}{2}\right)} \\ \times\int_0^{2\pi}d\theta_3 e^{-2i\frac{\sin(N\pi(\alpha_1-\alpha_3))}{\sin(\pi(\alpha_1-\alpha_3))}\sin\left(\frac{\theta_1+\theta_1^{'}}{2}-\theta_3+(N+1)\pi(\alpha_1-\alpha_3)\right)\sin\left(\frac{\theta_1^{'}-\theta_1}{2}\right)}\end{aligned} \tag{2.26}$$

This equation can be written as,

$$\rho_1(\theta_1,\theta_1^{'}) = C_1 J_0(C_2)J_0(C_3) \tag{2.27}$$

Where J_0 is the Bessel function of the first kind and C_1, C_2 and C_3 are constants w.r.t the integration such that,

$$C_1 = \frac{1}{2\pi}e^{ip_0^1(\theta_1-\theta_1^{'})}e^{-i\frac{\sin(N\pi\alpha_1)}{\sin(\pi\alpha_1)}\left[\cos(\theta_1+(N+1)\pi\alpha_1)-\cos\left(\theta_1^{'}+(N+1)\pi\alpha_1\right)\right]} \tag{2.28}$$

$$C_2 = 2\frac{\sin(N\pi(\alpha_1-\alpha_2))}{\sin(\pi(\alpha_1-\alpha_2))}\sin\left(\frac{\theta_1^{'}-\theta_1}{2}\right) \tag{2.29}$$

$$C_3 = 2\frac{\sin(N\pi(\alpha_1-\alpha_3))}{\sin(\pi(\alpha_1-\alpha_3))}\sin\left(\frac{\theta_1^{'}-\theta_1}{2}\right) \tag{2.30}$$

We can extend this equation for reduced density matrix for n-particles easily,

$$\rho_1(\theta_1,\theta_1^{'}) = C_1 J_0(C_2)J_0(C_3)\ldots J_0(C_n) \tag{2.31}$$

where the J_0 are Bessel functions of the first kind. Discretisation of this ρ_1 allows us to calculate $1\leftrightarrow(N-1)$ bipartite entanglement for any n number of particles.

2.1.3 The four cases of α_i for evolution of entanglement entropy

There are 4 cases for different values of α_i that affect the evolution of entanglement entropy corresponding to the localisation and delocalisation of momenta and energy for the n-particle system as described in the previous section.

- **Case 1: α_i are non-integers and $\alpha_i \neq \alpha_j$**

  For this case, both momenta of the n particles, as well as energy are localised. This is the case where we have complete localisation in the system. We have observed that the evolution of entanglement entropy for this case is periodic in time which agrees with the periodic momentum dynamics of the system.

- **Case 2: α_i are non-integers and $\alpha_1 = \alpha_2$ while $\alpha_2 ... \alpha_n$ are distinct**

  In this case, the momenta for particles 1 and 2 are delocalised while the energy as well as the momenta for the other particles are localised. We have observed that the entanglement entropy in this case shows a logarithmic increase. This evolution of entanglement entropy looks like what you would expect when we observe chaos, or delocalisation in the system.

- **Case 3: α_1 and α_2 are integers while $\alpha_3 ... \alpha_n$ are non-integers, and $\alpha_i \neq \alpha_j$**

  In this case, the momenta for particles 1 and 2 as well as the energy are delocalised. The entanglement entropy again shows logarithmic increase as in the previous case. This evolution of entanglement entropy also looks like what you would expect when we observe chaos, or delocalisation in the system.

- **Case 4: α_1 is an integer, $\alpha_2 ... \alpha_n$ are non-integers and $\alpha_i \neq \alpha_j$**

  In this case, the momentum for particle 1 and the energy are delocalised while the momenta for the other particles are localised. We have observed that the entanglement entropy in this case is periodic in time. This is a surprising case since we expected the entropy to increase logarithmically due to the delocalisation in the system, as we did in the previous two cases.

We looked at the math behind the four cases of evolution of entanglement entropy that we get, for different cases of α_i. We start with the evolution wave-function and, for simplicity and clarity, we proceed with the 3-particle case:

$$\begin{aligned}\Psi_N(\vec{\theta}) = e^{-i\sum_{n=1}^{N}[\cos(\theta_1-\theta_2+2\pi n(\alpha_1-\alpha_2))+\cos(\theta_2-\theta_3+2\pi n(\alpha_2-\alpha_3))+\cos(\theta_1-\theta_3+2\pi n(\alpha_1-\alpha_3))]} \\ \times e^{-i\sum_{n=1}^{N}[\cos(\theta_1+2\pi n\alpha_1)+\cos(\theta_2+2\pi n\alpha_2)+\cos(\theta_3+2\pi n\alpha_3)]} \times \psi_0(\vec{\theta})\end{aligned} \tag{2.32}$$

In this wave-function, we put in example values of α_i in accordance with the 4 cases above. Then the 4 cases for this wave-function equation are:

- **Case 1:** $\alpha_1 = 0.6,\ \alpha_2 = 0.5,\ \alpha_3 = 0.4$

$$\begin{aligned}\Psi_N(\vec{\theta}) = e^{-i\sum_{n=1}^{N}[\cos(\theta_1-\theta_2+2\pi n(0.1))+\cos(\theta_2-\theta_3+2\pi n(0.1))+\cos(\theta_1-\theta_3+2\pi n(0.2))]} \\ \times e^{-i\sum_{n=1}^{N}[\cos(\theta_1+2\pi n(0.6))+\cos(\theta_2+2\pi n(0.5))+\cos(\theta_3+2\pi n(0.4))]} \times \psi_0(\vec{\theta})\end{aligned} \tag{2.33}$$

- **Case 2:** $\alpha_1 = 0.5,\ \alpha_2 = 0.5,\ \alpha_3 = 0.4$

$$\begin{aligned}\Psi_N(\vec{\theta}) = e^{-i\sum_{n=1}^{N}[\cos(\theta_1-\theta_2)+\cos(\theta_2-\theta_3+2\pi n(0.1))+\cos(\theta_1-\theta_3+2\pi n(0.1))]} \\ \times e^{-i\sum_{n=1}^{N}[\cos(\theta_1+2\pi n(0.5))+\cos(\theta_2+2\pi n(0.5))+\cos(\theta_3+2\pi n(0.4))]} \times \psi_0(\vec{\theta})\end{aligned} \tag{2.34}$$

- **Case 3:** $\alpha_1 = 1,\ \alpha_2 = 2,\ \alpha_3 = 0.4$

$$\begin{aligned}\Psi_N(\vec{\theta}) = e^{-i\sum_{n=1}^{N}[\cos(\theta_1-\theta_2)+\cos(\theta_2-\theta_3+2\pi n(1.6))+\cos(\theta_1-\theta_3+2\pi n(0.6))]} \\ \times e^{-i\sum_{n=1}^{N}[\cos(\theta_1)+\cos(\theta_2)+\cos(\theta_3+2\pi n(0.4))]} \times \psi_0(\vec{\theta})\end{aligned} \tag{2.35}$$

- **Case 4:** $\alpha_1 = 1,\ \alpha_2 = 0.5,\ \alpha_3 = 0.4$

$$\begin{aligned}\Psi_N(\vec{\theta}) = e^{-i\sum_{n=1}^{N}[\cos(\theta_1-\theta_2+2\pi n(0.5))+\cos(\theta_2-\theta_3+2\pi n(0.1))+\cos(\theta_1-\theta_3+2\pi n(0.6))]} \\ \times e^{-i\sum_{n=1}^{N}[\cos(\theta_1)+\cos(\theta_2+2\pi n(0.5))+\cos(\theta_3+2\pi n(0.4))]} \times \psi_0(\vec{\theta})\end{aligned} \tag{2.36}$$

We have plotted the entanglement entropy for these 4 cases in Fig.(2.1).

From these cases, we see that for cases 2 and 3, where we observe logarithmic increase of entanglement entropy evolution, at least one of the interaction terms is independent of α_i. Whereas for cases 1 and 4, where the entanglement entropy evolution is periodic, there are no interaction terms independent of α_i. We explore further by looking at the Bessel function terms in the density matrix equation (2.27).

For cases 1 and 4 where α_1 and α_2 are as given above, the Bessel function $J_0(C_2)$ is found to be,

$$J_0(C_2) = \int_0^{2\pi} \frac{d\theta_2}{2\pi} \exp\left\{ i\left[\frac{2\sin(N\pi(\alpha_1-\alpha_2))}{\sin(\pi(\alpha_1-\alpha_2))} \sin\left(\frac{\theta_1'-\theta_1}{2}\right)\sin(\theta_2)\right]\right\} \tag{2.37}$$

$J_0(C_3)$ is similar to this but with α_3 instead of α_2.

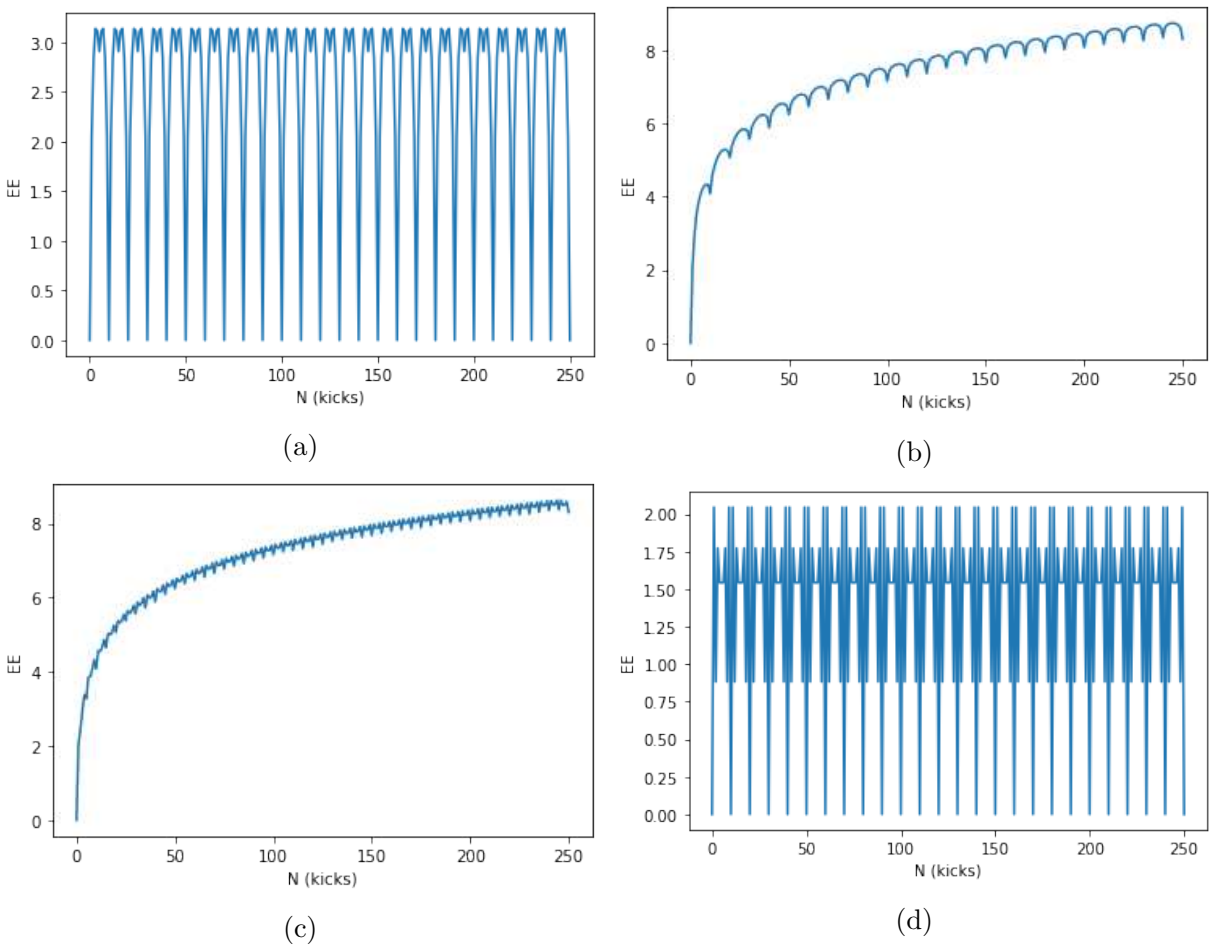

Figure 2.1: Entanglement entropy evolution plots corresponding to the 3-particle wavefunctions in the 4 example cases: (a)Case 1, (b)Case 2, (c)Case 3, (d)Case 4,

Whereas for α_i in cases 2 and 3, the Bessel function $J_0(C_2)$ is found to be,

$$J_0(C_2) = \int_0^{2\pi} \frac{d\theta_2}{2\pi} \exp\left\{ 2iN \sin\left(\frac{\theta_1' - \theta_1}{2} \right) \sin(\theta_2) \right\} \tag{2.38}$$

Therefore, mathematically, the logarithmic growth of the entanglement entropy evolution is caused for cases 2 and 3 due to the N in the exponent. As this Bessel function in turn enters the logarithm in the entropy equation (2.22), we get the dynamics that we observe. For the cases 1 and 4, the N is replaced by a sinusoidal term because of which the entire exponent is filled with sinusoidal terms. This leads to the periodicity that we observe when this Bessel function is entered into the entropy equation.

Physically we can can say that, for case 1, the entanglement entropy is periodic since the entire system is localised and shows periodic dynamics. For cases 2 and 3, the entanglement entropy dynamics follows what we expect for delocalised systems, which is a logarithmic increase. Case 4, which shows periodic entanglement entropy dynamics despite delocalisation in one of the particles in the system, has been explained mathematically above but we have not been able to explain it physically.

2.1.4 Calculating the entanglement entropy for the quasi-energy wave-function (2-particles)

For the 2-particle system with the Hamiltonian given in equation (1.8), the quasi-energy wave-function is given by,

$$\Psi_\omega(\theta_1, \theta_2) = \frac{1}{2\pi} \exp\left\{ i\vec{M}.\vec{\theta} - \frac{i}{2} \frac{\sin(\theta_1 + \pi\alpha_1)}{\sin(\pi\alpha_1)} - \frac{i}{2} \frac{\sin(\theta_2 + \pi\alpha_2)}{\sin(\pi\alpha_2)} - \frac{i}{2} \frac{\sin(\theta_1 - \theta_2)}{\pi(\alpha_1 - \alpha_2)} \right\} \tag{2.39}$$

Where ω are the quasi-energy eigenvalues corresponding to these wave-functions and are given as,

$$\omega = 2\pi\vec{\alpha}.\vec{M} \quad mod(2\pi) \tag{2.40}$$

Here, M_1 and M_2 are any arbitrary integers.

In terms of ω, the quasi-energy wave-function can be written as,

$$\Psi_{\omega}(\theta_1,\theta_2)=\frac{1}{2\pi}\exp\Bigg\{\frac{i\omega\theta_1}{2\pi\alpha_1}+\frac{i\omega\theta_2}{2\pi\alpha_2}-\frac{i}{2}\frac{\sin(\theta_1+\pi\alpha_1)}{\sin(\pi\alpha_1)}-\frac{i}{2}\frac{\sin(\theta_2+\pi\alpha_2)}{\sin(\pi\alpha_2)}-\frac{i}{2}\frac{\sin(\theta_1-\theta_2)}{\pi(\alpha_1-\alpha_2)}\Bigg\} \tag{2.41}$$

The reduced density matrix kernel for the first particle is given by (2.9) and, for this wave-function, it becomes,

$$\rho_1(\theta_1,\theta_1^{'})=\int_0^{2\pi}d\theta_2\frac{1}{(2\pi)^2}\exp\Bigg\{\frac{i\omega}{2\pi\alpha_1}(\theta_1-\theta_1^{'})-\frac{i}{2\sin(\pi\alpha_1)}\Bigg[\sin(\theta_1+\pi\alpha_1)-\sin\Big(\theta_1^{'}+\pi\alpha_1\Big)\Bigg]\Bigg\}$$
$$\times\exp\Bigg\{-\frac{i}{2\pi(\alpha_1-\alpha_2)}\Bigg[\sin(\theta_1-\theta_2)-\sin\Big(\theta_1^{'}-\theta_2\Big)\Bigg]\Bigg\} \tag{2.42}$$

From trigonometric identities, we get,

$$\sin(\theta_1-\theta_2)-\sin\Big(\theta_1^{'}-\theta_2\Big)=2\cos\Bigg(\frac{\theta_1+\theta_1^{'}}{2}-\theta_2\Bigg)\sin\Bigg(\frac{\theta_1-\theta_1^{'}}{2}\Bigg) \tag{2.43}$$

The reduced density matrix then becomes,

$$\rho_1(\theta_1,\theta_1^{'})=\int_0^{2\pi}d\theta_2\frac{1}{(2\pi)^2}\exp\Bigg\{\frac{i\omega}{2\pi\alpha_1}(\theta_1-\theta_1^{'})-\frac{i}{2\sin(\pi\alpha_1)}\Bigg[\sin(\theta_1+\pi\alpha_1)-\sin\Big(\theta_1^{'}+\pi\alpha_1\Big)\Bigg]\Bigg\}$$
$$\times\exp\Bigg\{\frac{i}{\pi(\alpha_1-\alpha_2)}\cos\Bigg(\frac{\theta_1+\theta_1^{'}}{2}-\theta_2\Bigg)\sin\Bigg(\frac{\theta_1^{'}-\theta_1}{2}\Bigg)\Bigg\} \tag{2.44}$$

This can be written in simplified form as,

$$\rho_1(\theta_1,\theta_1^{'})=\int_0^{2\pi}\frac{d\theta_2}{2\pi}C_1e^{iC_2\sin(\theta_2)}=C_1J_0(C_2) \tag{2.45}$$

Where J_0 is the bessel function of the first kind and C_1 and C_2 are constants w.r.t the integration and are such that,

$$C_1=\frac{1}{2\pi}\exp\Bigg\{\frac{i\omega}{2\pi\alpha_1}(\theta_1-\theta_1^{'})-\frac{i}{2\sin(\pi\alpha_1)}\Bigg[\sin(\theta_1+\pi\alpha_1)-\sin\Big(\theta_1^{'}+\pi\alpha_1\Big)\Bigg]\Bigg\} \tag{2.46}$$

$$C_2=\frac{1}{\pi(\alpha_1-\alpha_2)}\sin\Bigg(\frac{\theta_1^{'}-\theta_1}{2}\Bigg) \tag{2.47}$$

This reduced density matrix can be discretised to get its eigenvalues and from that we can

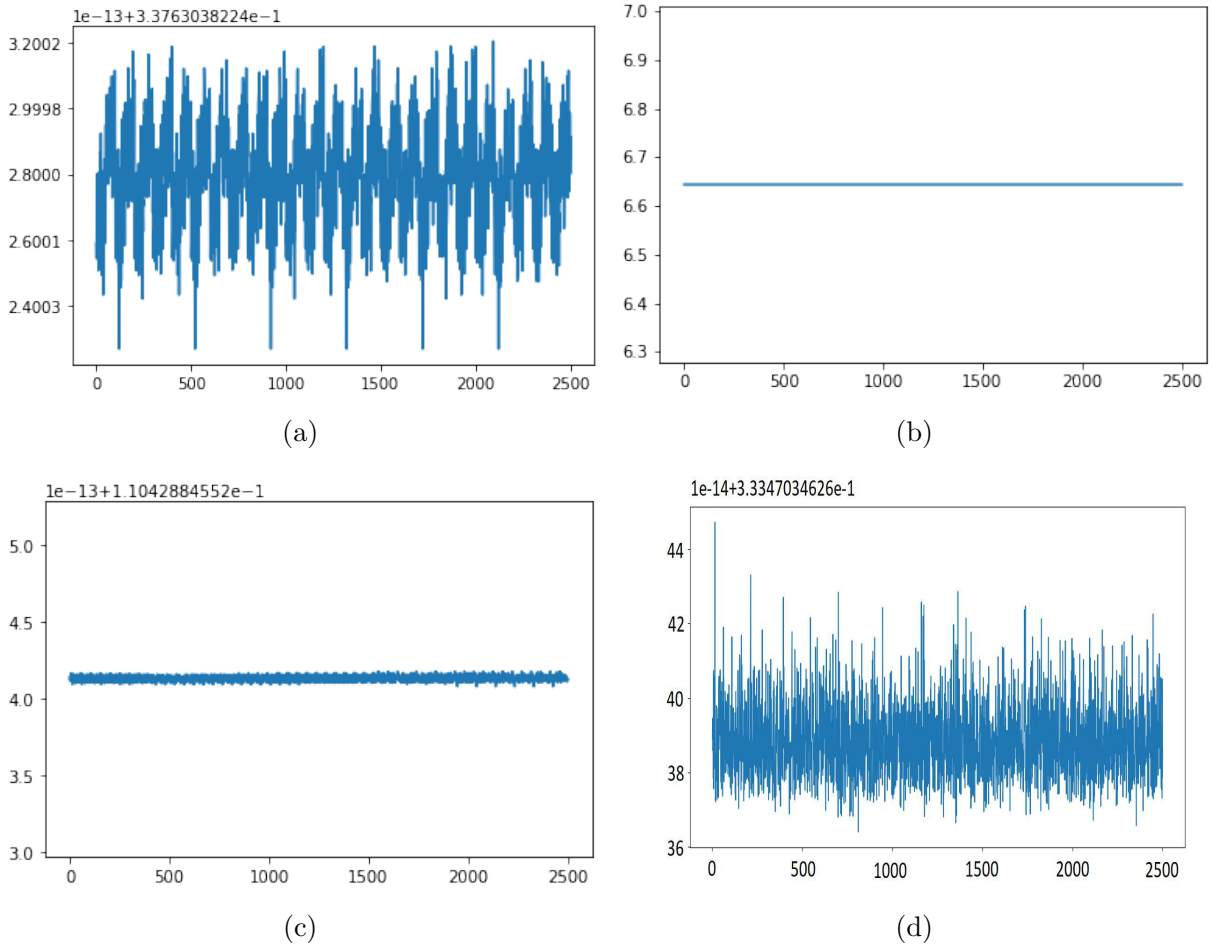

Figure 2.2: Entanglement entropy plots corresponding to the quasi-energy wave-functions for the 4 cases of α_i. As can be observed, all four of the plots show a constant entropy for 2500 eigenvalues of the system, the particular value of the constant being different for the 4 plots due to difference in values of α_i.(b)Entropy is clearly a constant value line. (a,c,d)Entropy is still constant since the variations on the plot are of the order of 10^{-13} and 10^{-14} which is outside the precision we are considering.

calculate the entanglement entropy according to the equation (2.22)

We have plotted the entanglement entropy corresping to the quasi-energy eigenvalues in Fig.(2.2). From the plots we observe that the entanglement entropy remains constant for all the quasi-energy eigenstates corresponding to the different eigenvalues of the system. The value of these constants is seen to be dependent on the values of the parameters α_i. The constant values for entanglement entropy seem to suggest a thermalisation happening in the system for the quasi-energy eigenstates.

2.2 Information Entropy for the Quantum Linear Kicked Rotor System

Information entropy of a system is calculated as,

$$S = -|\Psi|^2 \log \left|\Psi^2\right| \tag{2.48}$$

For the system at hand, we calculate the information entropy for both the evolution and quasi-energy wave-functions.

The evolution wave-function of the system is given by,

$$\Psi_N(\theta_1, \theta_2) = e^{-i\sum_{n=1}^{N}[\cos(\theta_1+2\pi n\alpha_1)+\cos(\theta_2+2\pi n\alpha_2)+\cos(\theta_1-\theta_2+2\pi n(\alpha_1-\alpha_1))]}\psi_0(\theta_1, \theta_2) \tag{2.49}$$

Where,

$$\psi_0(\theta_1, \theta_2) = \frac{1}{2\pi} e^{i(p_0^1\theta_1+p_0^2\theta_2)} \tag{2.50}$$

For this wave-function,

$$|\Psi|^2 = \frac{1}{(2\pi)^2} \tag{2.51}$$

Which gives the information entropy for the wave-function as,

$$S = \frac{1}{2\pi^2} \log(2\pi) \tag{2.52}$$

Moving on to the quasi-energy wave-function for this system, it is given by,

$$\Psi_{\omega}(\theta_1, \theta_2) = \frac{1}{2\pi}\exp\left\{ \frac{i\omega\theta_1}{2\pi\alpha_1} + \frac{i\omega\theta_2}{2\pi\alpha_2} - \frac{i}{2}\frac{\sin(\theta_1 + \pi\alpha_1)}{\sin(\pi\alpha_1)} - \frac{i}{2}\frac{\sin(\theta_2 + \pi\alpha_2)}{\sin(\pi\alpha_2)} - \frac{i}{2}\frac{\sin(\theta_1 - \theta_2)}{\pi(\alpha_1 - \alpha_2)} \right\} \tag{2.53}$$

For this wave-function as well,

$$|\Psi|^2 = \frac{1}{(2\pi)^2} \tag{2.54}$$

Which gives the information entropy for the wave-function as,

$$S = \frac{1}{2\pi^2}\log(2\pi) \tag{2.55}$$

Therefore we see that unlike entanglement entropy, information entropy for the linear kicked rotor system is always constant and equal for both the evolution as well as quasi-energy wave-function and are independent of parameters of the system. This happening because the dynamics of the system is completely phase dependent. As such, this information entropy doesn't really tell us much about the system.

Chapter 3

Classical Dynamics for the Linear Kicked Rotor System

The classical linear kicked rotor system is an exactly solvable system which makes it an exceptional case among kicked rotors. It is also interesting in that the dynamics observed for both the classical and quantum versions of this system show exact correspondence. We have shown this correspondence explicitly in the dynamics. We have also shown the absence of chaos in the system.

The Hamiltonian for the classical interacting linear kicked rotor for the 2-particle case is,

$$H = 2\pi\alpha_1 p_1 + 2\pi\alpha_2 p_2 + \cos(\theta_1 - \theta_2) + [\cos(\theta_1) + \cos(\theta_2)] \sum_{n=-\infty}^{\infty} \delta(t - n) \tag{3.1}$$

Where, $0 \leq \theta_i < 2\pi$ and $-\infty < p_i < \infty$

The system can be thought of as two interacting particles on a ring, moving with constant speed $2\pi\alpha_1$ and $2\pi\alpha_2$ respectively. The particles complete α_i orbits between each successive kick.

The equations of motion for this system can be written as the discrete map,

$$\theta_1^{n+1} = \theta_1^n + 2\pi\alpha_1, \qquad p_1^{n+1} = p_1^n + \sin\left(\theta_1^{n+1}\right) + \sin\left(\theta_1^{n+1} - \theta_2^{n+1}\right) \tag{3.2}$$

$$\theta_2^{n+1} = \theta_2^n + 2\pi\alpha_2, \qquad p_2^{n+1} = p_2^n + \sin\big(\theta_2^{n+1}\big) - \sin\big(\theta_1^{n+1} - \theta_2^{n+1}\big) \tag{3.3}$$

Using trigonometric identity,

$$\sin\big(\theta_1^{n+1}\big) = \frac{\cos(\theta_1^n + \pi\alpha_1) - \cos\big(\theta_1^{n+1} + \pi\alpha_1\big)}{2\sin(\pi\alpha_1)} \tag{3.4}$$

Using this, the momentum evolution equations become,

$$\begin{aligned} p_1^{n+1} + \frac{\cos\big(\theta_1^{n+1} + \pi\alpha_1\big)}{2\sin(\pi\alpha_1)} + \frac{\cos\big(\theta_1^{n+1} - \theta_2^{n+1} + \pi(\alpha_1 - \alpha_2)\big)}{2\sin(\pi(\alpha_1 - \alpha_2))} \\ = p_1^n + \frac{\cos(\theta_1^n + \pi\alpha_1)}{2\sin(\pi\alpha_1)} + \frac{\cos(\theta_1^n - \theta_2^n + \pi(\alpha_1 - \alpha_2))}{2\sin(\pi(\alpha_1 - \alpha_2))} \end{aligned} \tag{3.5}$$

and,

$$\begin{aligned} p_2^{n+1} + \frac{\cos\big(\theta_2^{n+1} + \pi\alpha_2\big)}{2\sin(\pi\alpha_2)} - \frac{\cos\big(\theta_1^{n+1} - \theta_2^{n+1} + \pi(\alpha_1 - \alpha_2)\big)}{2\sin(\pi(\alpha_1 - \alpha_2))} \\ = p_2^n + \frac{\cos(\theta_2^n + \pi\alpha_2)}{2\sin(\pi\alpha_2)} - \frac{\cos(\theta_1^n - \theta_2^n + \pi(\alpha_1 - \alpha_2))}{2\sin(\pi(\alpha_1 - \alpha_2))} \end{aligned} \tag{3.6}$$

From this, we can see that each side of the equation for both the momenta are constants of motion, say, K_1 and K_2. Therefore we can write invariant curves for the two momenta as,

$$p_1^n = K_1 - \frac{\cos(\theta_1^n + \pi\alpha_1)}{2\sin(\pi\alpha_1)} - \frac{\cos(\theta_1^n - \theta_2^n + \pi(\alpha_1 - \alpha_2))}{2\sin(\pi(\alpha_1 - \alpha_2))} \tag{3.7}$$

and

$$p_2^n = K_2 - \frac{\cos(\theta_2^n + \pi\alpha_2)}{2\sin(\pi\alpha_2)} + \frac{\cos(\theta_1^n - \theta_2^n + \pi(\alpha_1 - \alpha_2))}{2\sin(\pi(\alpha_1 - \alpha_2))} \tag{3.8}$$

These two invariant curves exist so long as α_1, α_2 and $(\alpha_1 - \alpha_2)$ are not integers.

Given the intial conditions of the system as θ_1^0, θ_2^0, p_1^0 and p_2^0, we can write the equations immediately after nth kick as,

$$\theta_1^n = \theta_1^0 + 2\pi n\alpha_1, \qquad \theta_2^n = \theta_2^0 + 2\pi n\alpha_2 \tag{3.9}$$

$$p_1^n = p_1^0 + \frac{\sin[\theta_1^0 + \pi\alpha_1(n+1)]\sin(n\pi\alpha_1)}{\sin(\pi\alpha_1)} + \frac{\sin[\theta_1^0 - \theta_2^0 + \pi(\alpha_1 - \alpha_2)(n+1)]\sin[n\pi(\alpha_1 - \alpha_2)]}{\sin[\pi(\alpha_1 - \alpha_2)]} \tag{3.10}$$

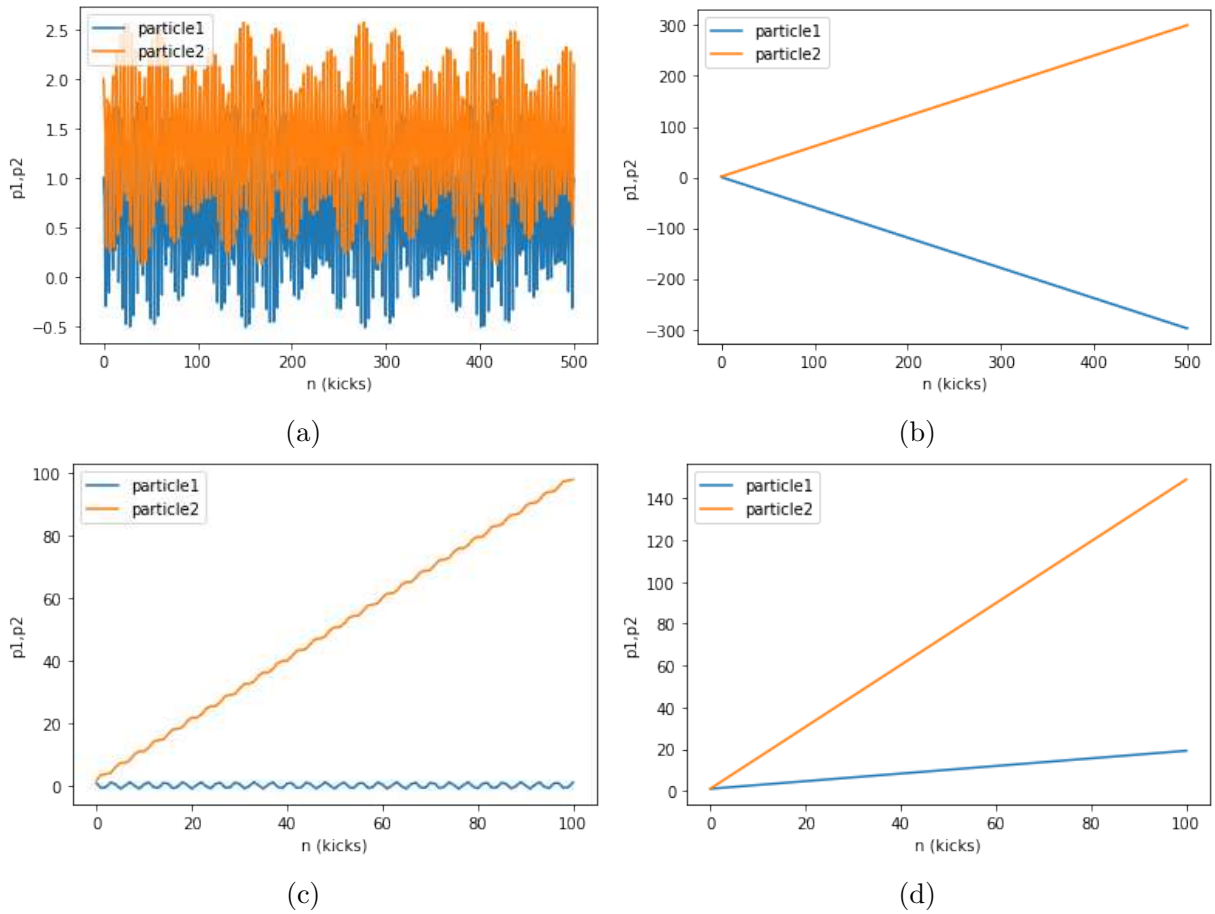

Figure 3.1: Momentum evolution for the 4 cases of α_i. (a) $\alpha_1 = \sqrt{3}$, $\alpha_2 = \sqrt{5}$, (b) $\alpha_1 = \sqrt{3}$, $\alpha_2 = \sqrt{3}$, (c) $\alpha_1 = \sqrt{3}$, $\alpha_2 = 1$, (d) $\alpha_1 = 2$, $\alpha_2 = 1$

$$p_2^n = p_2^0 + \frac{\sin[\theta_2^0 + \pi\alpha_2(n+1)]\sin(n\pi\alpha_2)}{\sin(\pi\alpha_2)} - \frac{\sin[\theta_1^0 - \theta_2^0 + \pi(\alpha_1 - \alpha_2)(n+1)]\sin[n\pi(\alpha_1 - \alpha_2)]}{\sin[\pi(\alpha_1 - \alpha_2)]} \tag{3.11}$$

We have plotted these evolution equations for p_i (Fig.(3.1)) as well as an evolution equation for the Hamiltonian H_n (Fig.(3.2)) from equation (3.1). We see that the both the momenta of particles 1 and 2 as well as the Hamiltonian have localised and delocalised regimes governed by values of parameters α_i that correspond exactly to the localised and delocalised regimes of the quantum system for these same α_i.

We have further plotted the Poincare sections for particles 1 and 2 (Fig.(3.3) and Fig.(3.4)) which show clearly that there is no chaos for this system and that it is completely integrable.

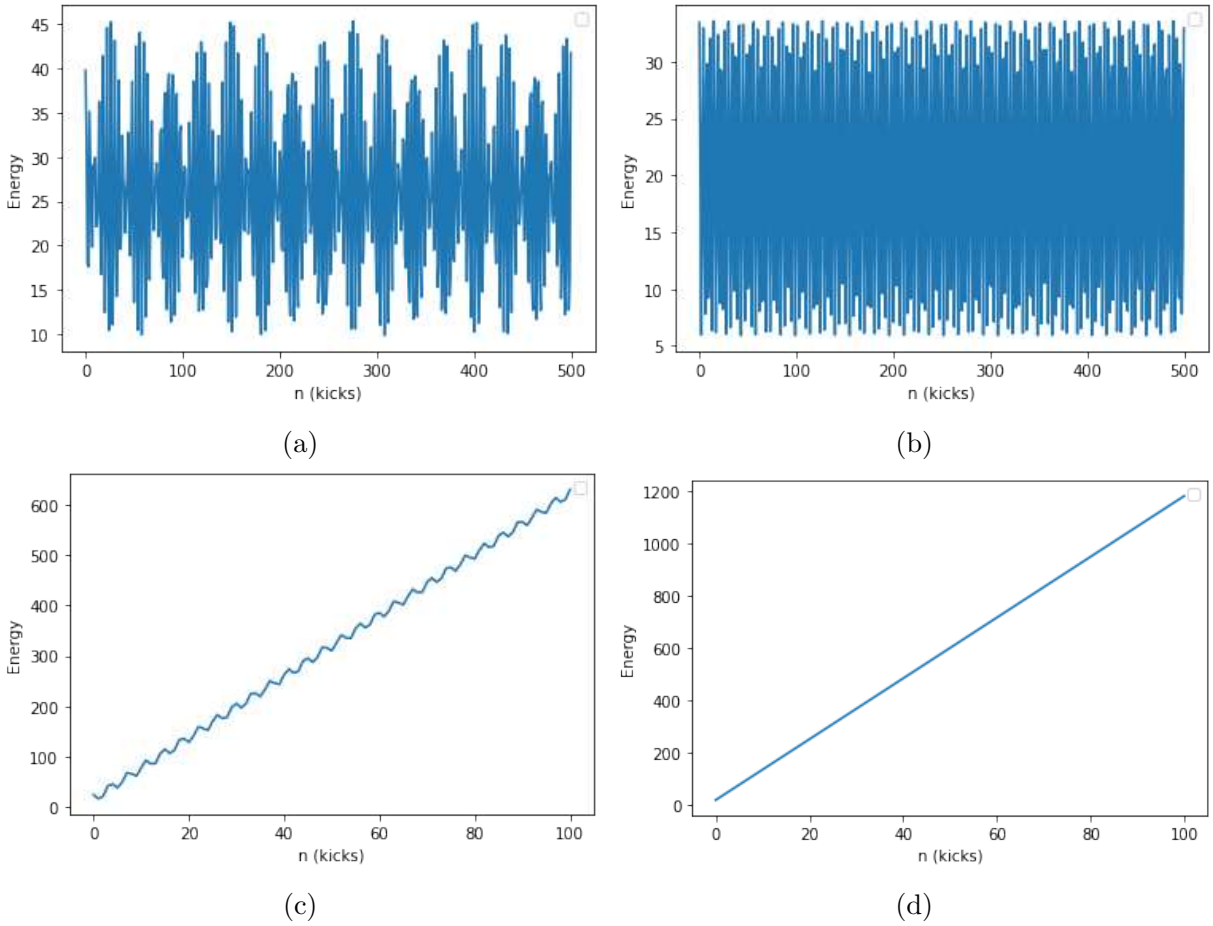

Figure 3.2: Energy(Hamiltonian) evolution for the 4 cases of α_i. (a) $\alpha_1 = \sqrt{3}$, $\alpha_2 = \sqrt{5}$, (b) $\alpha_1 = \sqrt{3}$, $\alpha_2 = \sqrt{3}$, (c) $\alpha_1 = \sqrt{3}$, $\alpha_2 = 1$, (d) $\alpha_1 = 2$, $\alpha_2 = 1$

One thing of note for this system is that the Hamiltonian of this system is a form of potential energy for this system. So the plots here are for this 'potential energy' and not for the kinetic energy or in fact the total energy of the system. For this reason, this quantity can also be negative.

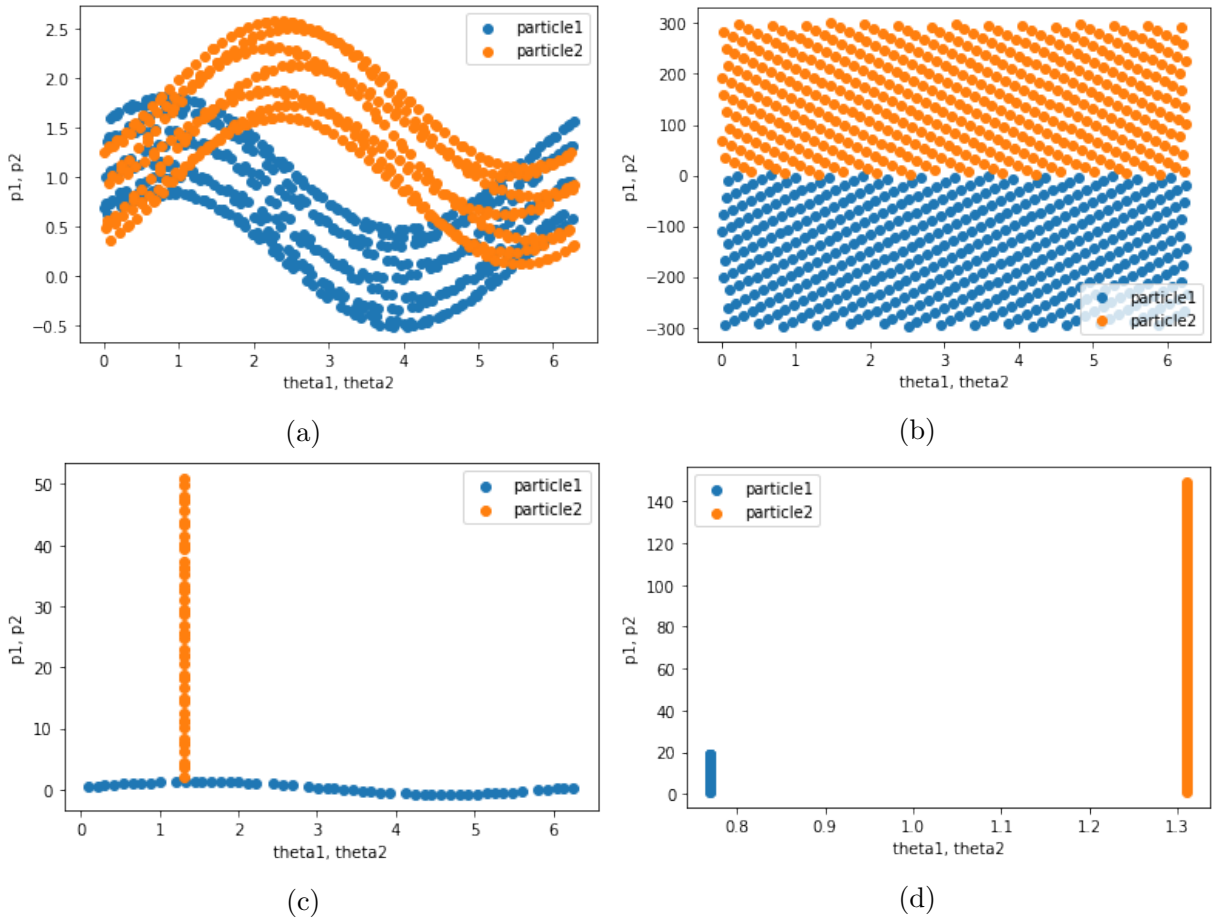

Figure 3.3: Poincare sections for the 4 cases of α_i. (a) $\alpha_1 = \sqrt{3}$, $\alpha_2 = \sqrt{5}$, (b) $\alpha_1 = \sqrt{3}$, $\alpha_2 = \sqrt{3}$, (c) $\alpha_1 = \sqrt{3}$, $\alpha_2 = 1$, (d) $\alpha_1 = 2$, $\alpha_2 = 1$

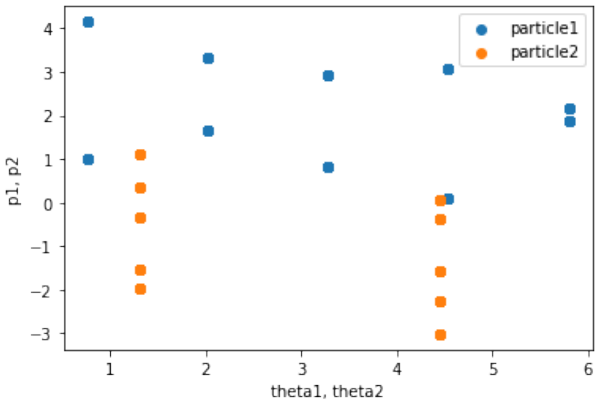

(a)

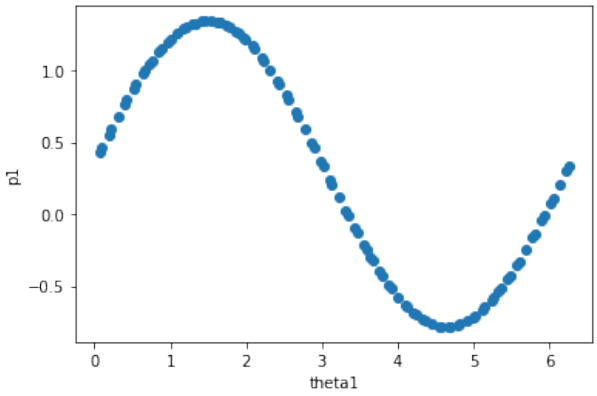

(b)

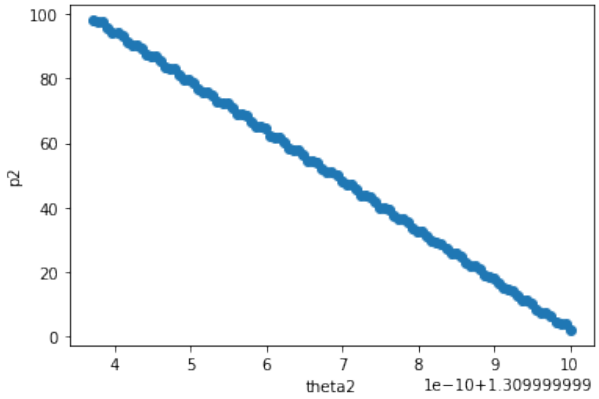

(c)

Figure 3.4: (a)Poincare section when $\alpha_1 = 0.6$, $\alpha_2 = 0.5$.(b) and (c) are Poincare sections for particles 1 and 2 respectively when $\alpha_1 = \sqrt{3}$ and $\alpha_2 = 1$. It is the same plot as Fig. 3.3 (c) but with the Poincare section for each particle enlarged. The above figure (c) shows that while the Poincare section is constant for particle 1 when α is an integer, there is still a minuscule variation in that constant of the order of 10^{-10}

Chapter 4

Inducing Chaos in the Linear Kicked Rotor System

Given that the system we were considering so far showed no transition to chaos, quantum or classical, irrespective of kicking strength, we have tried inducing chaos into the classical system and looked at how this changes the quantum case.

4.1 Classical mechanics

The Hamiltonian for the classical 2-particle system is,

$$H = 2\pi\alpha_1 p_1 + 2\pi\alpha_2 p_2 + k_t \cos(\theta_1 - \theta_2) + k_p \cos(p_1 - p_2) + K[\cos(\theta_1) + \cos(\theta_2)] \sum_{n=-\infty}^{\infty} \delta(t - n) \tag{4.1}$$

Where $0 \leq \theta_i < 2\pi$ and $-\infty < p_i < \infty$. The position and momentum evolution equations then are,

$$\theta_1^{n+1} = \theta_1^n + 2\pi\alpha_1 - k_p \sin(p_1^n - p_2^n), \qquad p_1^{n+1} = p_1^n + K \sin\left(\theta_1^{n+1}\right) + k_t \sin\left(\theta_1^{n+1} - \theta_2^{n+1}\right) \tag{4.2}$$

$$\theta_2^{n+1} = \theta_2^n + 2\pi\alpha_2 + k_p \sin(p_1^n - p_2^n), \qquad p_2^{n+1} = p_2^n + K \sin\left(\theta_2^{n+1}\right) - k_t \sin\left(\theta_1^{n+1} - \theta_2^{n+1}\right) \tag{4.3}$$

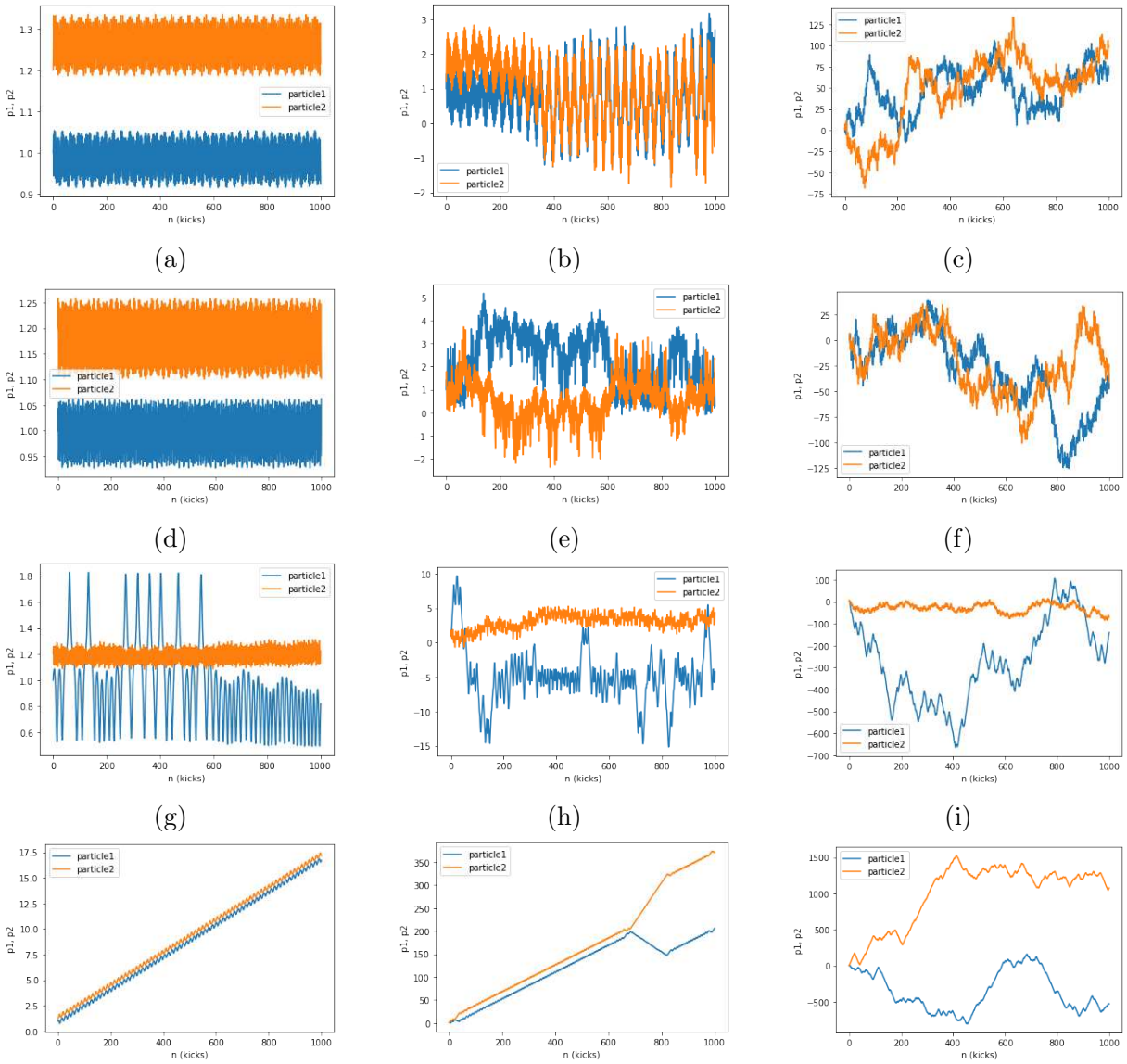

Figure 4.1: Momentum evolution for the 4 cases of α_i with increasing kicking strength K. (a - c) $\alpha_1 = \sqrt{3}$, $\alpha_2 = \sqrt{5}$, $K = 0.1, 1, 10$ for (a), (b), (c) respectively. (d - f) $\alpha_1 = \sqrt{3}$, $\alpha_2 = \sqrt{3}$, $K = 0.1, 1, 10$ for (d), (e), (f) respectively. (g - i) $\alpha_1 = 1$, $\alpha_2 = \sqrt{3}$, $K = 0.1, 1, 10$ for (g), (h), (i) respectively. (j-l) $\alpha_1 = 1$, $\alpha_2 = 3$, $K = 0.1, 1, 10$ for (j), (k), (l) respectively.

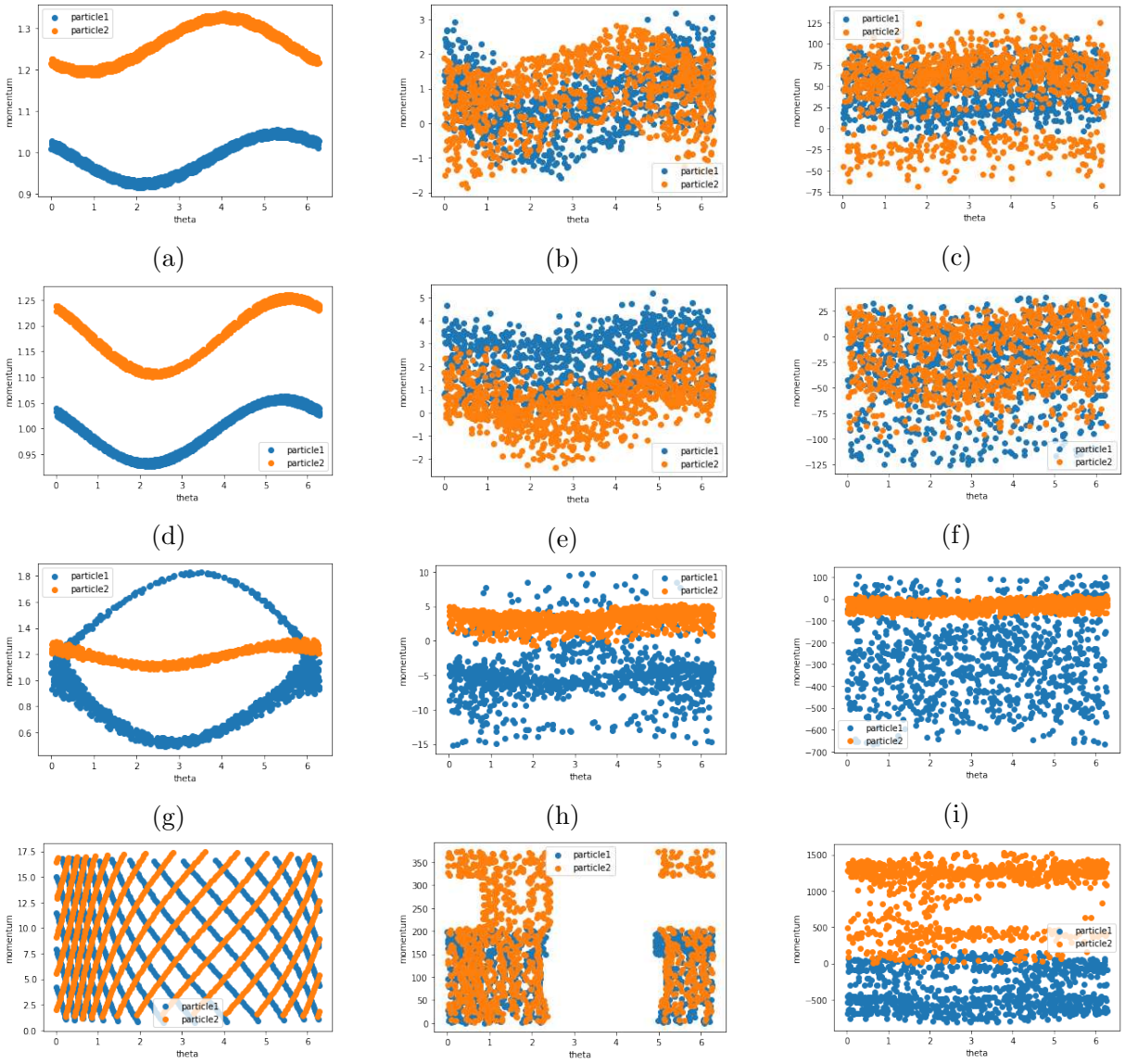

Figure 4.2: Poincare section for the 4 cases of α_i with increasing kicking strength K. (a - c) $\alpha_1 = \sqrt{3}$, $\alpha_2 = \sqrt{5}$, $K = 0.1, 1, 10$ for (a), (b), (c) respectively. (d - f) $\alpha_1 = \sqrt{3}$, $\alpha_2 = \sqrt{3}$, $K = 0.1, 1, 10$ for (d), (e), (f) respectively. (g - i) $\alpha_1 = 1$, $\alpha_2 = \sqrt{3}$, $K = 0.1, 1, 10$ for (g), (h), (i) respectively. (j-l) $\alpha_1 = 1$, $\alpha_2 = 3$, $K = 0.1, 1, 10$ for (j), (k), (l) respectively.

We have plotted the momentum evolution (Fig.(4.1)) for the system as well as the Poincare section (Fig.(4.2)) for these evolution equations and we observe a transition from periodic to non periodic (chaotic) evolution for increasing values of kicking strength K, with $k_p = 1$ and $k_t = 0$. To explore this further, we calculate the power spectrum as well as the lyapunov exponents of the system.

4.1.1 Power Spectrum

Power spectrum for any system is one of the ways we can check for regular or chaotic dynamics in the system. We do this by looking at the form of the spectrum.

If the system shows regular dynamics, the power spectrum will show distinct peaks which correspond to fundamental frequencies or some combinations of these frequencies. The spectrum may also have a predictability to the height and width of the peaks. The height of the peaks for regular dynamics increases as the time T increases. The width of the peaks decreases as the time T increases.

If the system shows chaotic dynamics, the power spectrum ceases to have predictability. The spectrum becomes "grassy" and we become unable to distinguish between specific frequency peaks. Certain peaks may even split up into multiple sub-peaks. In fact, we may see many peaks that are not properly separated from each other. Some of the peaks in the spectrum also cease to persist as the time T is increased to a large enough value.

The power spectrum for a system can be found as the Fourier transform of the auto-correlation function. We, however, have found the power spectrum directly from the momentum function with respect to time.

If we have a function of time, like the evolution equations for our system, $x(t)$, the energy contained in that function or wave can be written as an integration over time t of the absolute value of the function squared. That is,

$$E = \int_{-\infty}^{\infty} dt|x(t)|^2 \tag{4.4}$$

Given this equation, it has been shown that,

$$\int_{-\infty}^{\infty} dt|x(t)|^2 = \int_{-\infty}^{\infty} df|X(f)|^2 \tag{4.5}$$

This $|X(f)|^2$ is then equal to the energy density of the wave over the frequency. This energy density is also knows as power spectral density, or simply, power spectrum.

Therefore, to calculate the power spectrum for our system directly, we calculate it as the absolute value squared of the Fourier transform of the momentum evolution functions of our system.

For particle 1,

$$p_1^{n+1} = g_1(\theta_1^n, \theta_2^n, p_1^n, p_2^n) \tag{4.6}$$

If the Fourier transform of this function $g_1(\theta_1^n, \theta_2^n, p_1^n, p_2^n)$ is given as $P_1(f)$ where f is the frequency or $1/n$, then the power spectrum is calculated as,

$$Power\ spectrum = |P_1(f)|^2 \tag{4.7}$$

Similarly for particle 2, the power spectrum is given as,

$$Power\ spectrum = |P_2(f)|^2 \tag{4.8}$$

Where $P_2(f)$ is the Fourier transform of

$$p_2^{n+1} = g_2(\theta_1^n, \theta_2^n, p_1^n, p_2^n) \tag{4.9}$$

We have plotted the power spectrum for the system for different values of α_i as well as K (kicking strength) with fixed values, $k_p = 1$ and $k_t = 0$. For each of the 4 cases of α_i, we have plotted 3 figures each for both particle 1 and particle 2 corresponding to different values of K, Fig.(4.3)-(4.6). From these plots we can see that the spectrum has distinct peaks for $K = 0.1$ but as we increase the value of K, the spectrum becomes more and more "grassy", thereby showing a transition into chaos for the system.

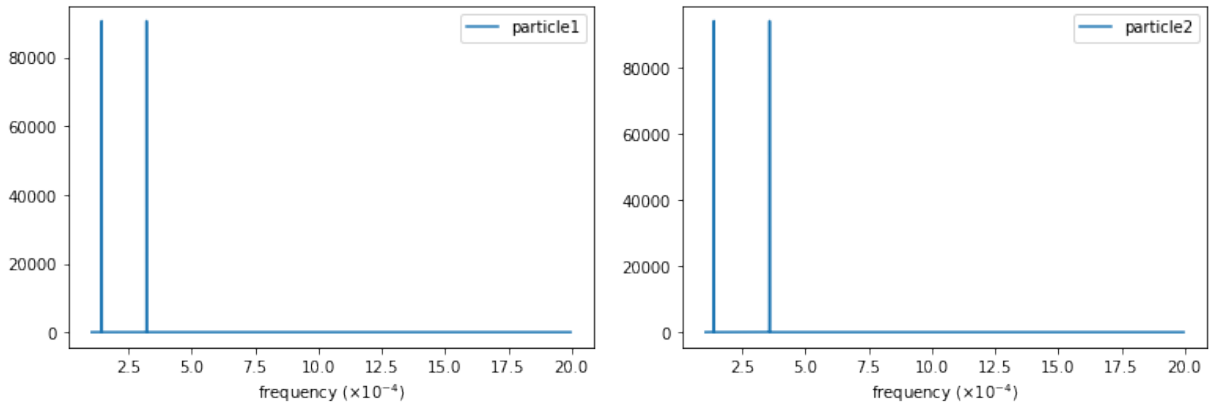

(a)

(b)

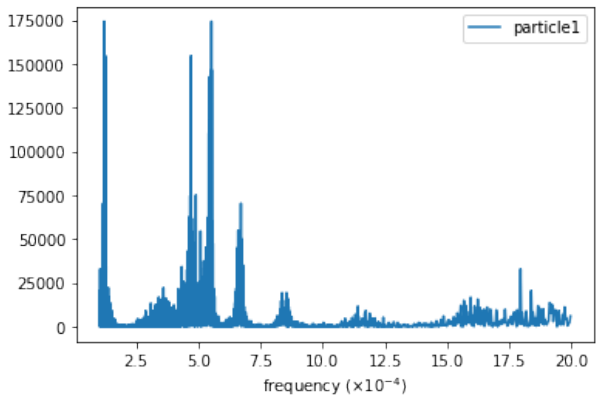

(c)

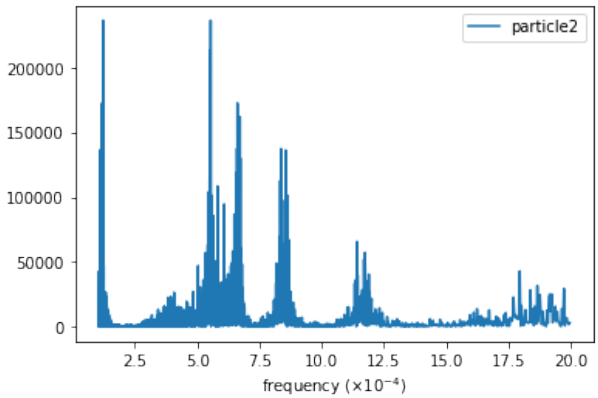

(d)

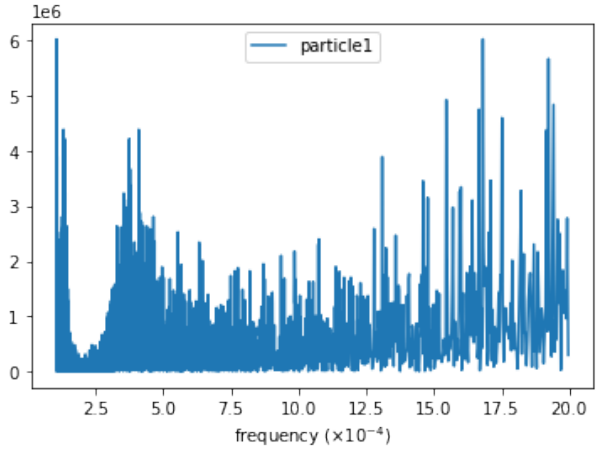

(e)

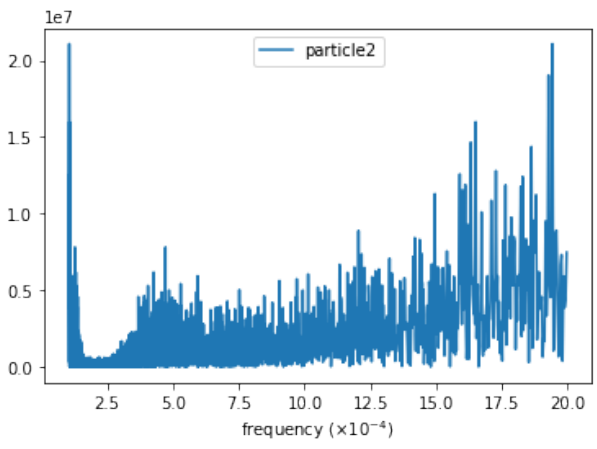

(f)

Figure 4.3: power spectrum for particle 1 and 2 for $\alpha_1 = \sqrt{3}$ and $\alpha_2 = \sqrt{5}$. (a),(b) $K = 0.1$; (c),(d) $K = 1$; (e),(f) $K = 10$.

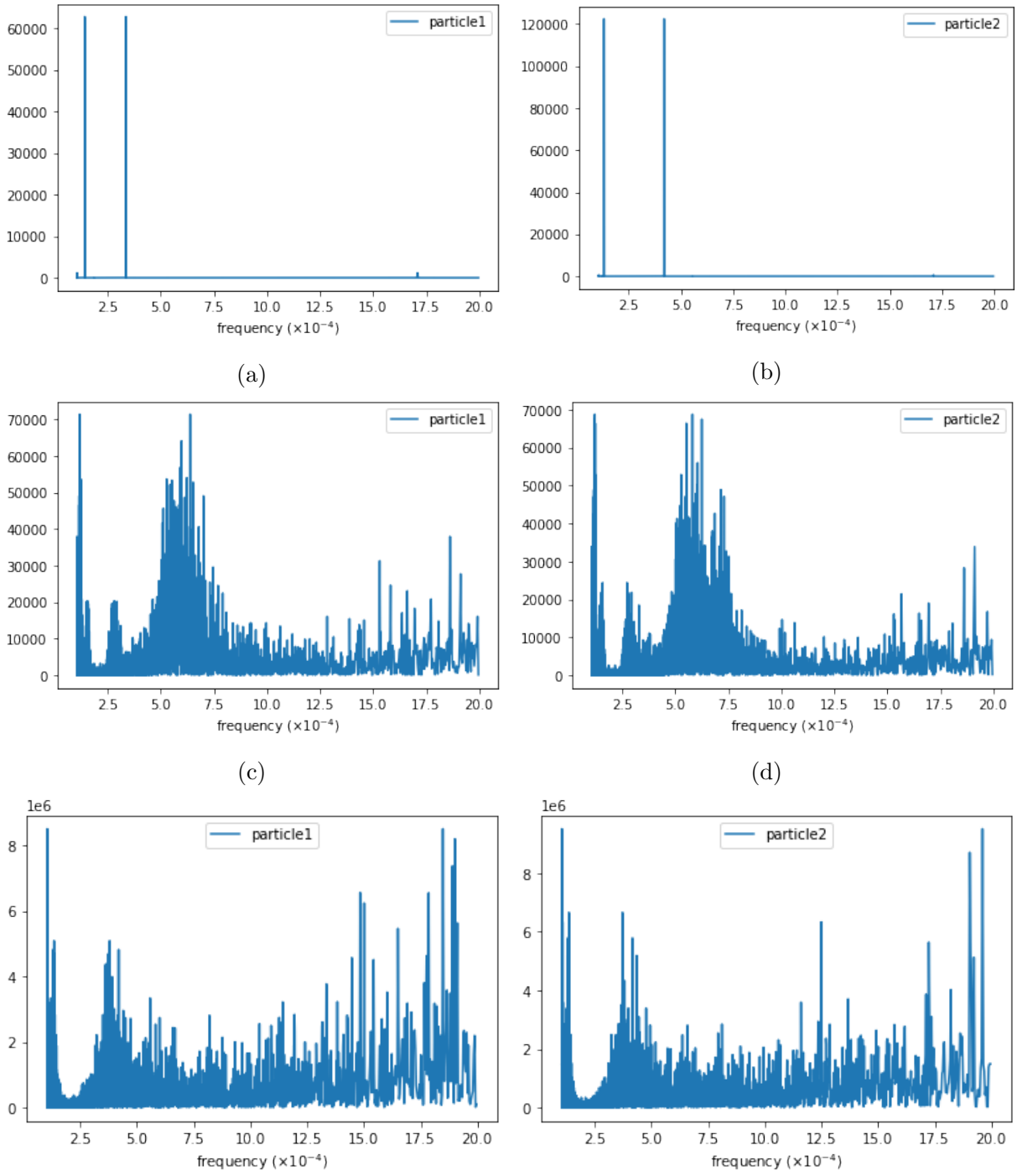

Figure 4.4: power spectrum for particle 1 and 2 for $\alpha_1 = \sqrt{3}$ and $\alpha_2 = \sqrt{3}$. (a),(b) $K = 0.1$; (c),(d) $K = 1$; (e),(f) $K = 10$.

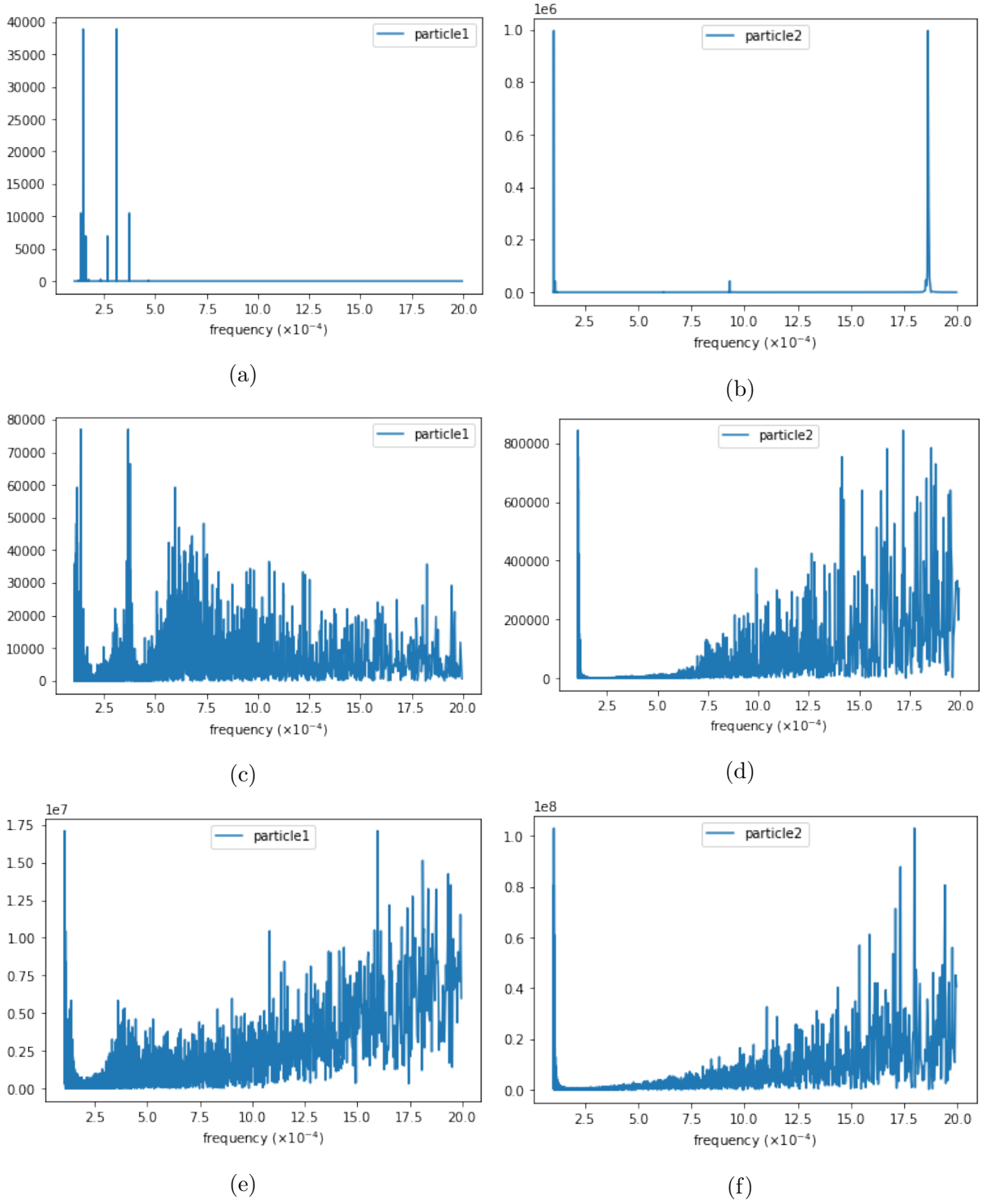

Figure 4.5: power spectrum for particle 1 and 2 for $\alpha_1 = \sqrt{3}$ and $\alpha_2 = 1$. (a),(b) $K = 0.1$; (c),(d) $K = 1$; (e),(f) $K = 10$.

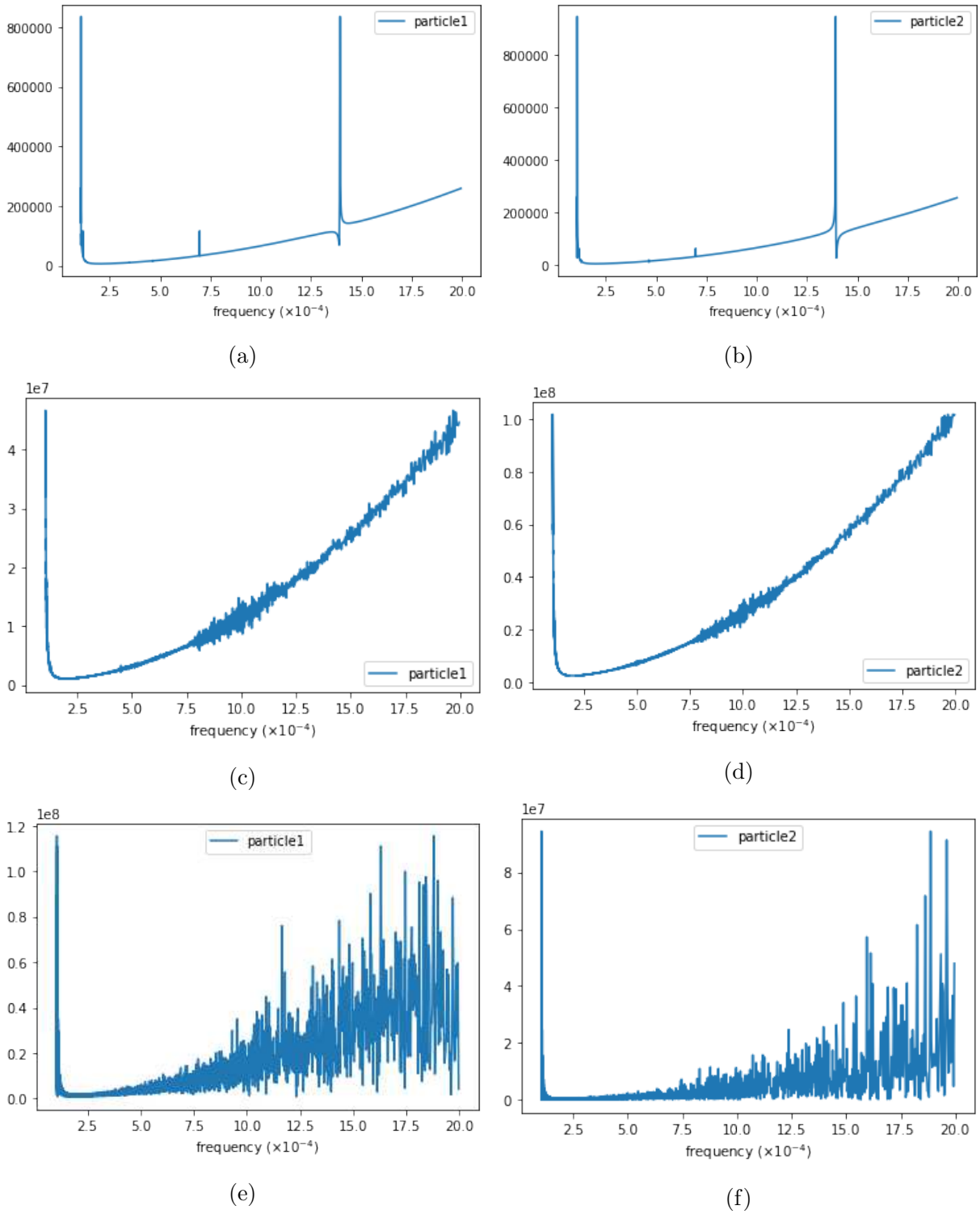

Figure 4.6: power spectrum for particle 1 and 2 for $\alpha_1 = 2$ and $\alpha_2 = 1$. (a),(b) $K = 0.1$; (c),(d) $K = 1$; (e),(f) $K = 10$.

4.1.2 Lyapunov Exponent

The separation between two trajectories, that start out infinitesimally close, can increase or decrease exponentially. The Lyapunov exponents of the system are then quantities that represent this rate of seperation.

Consider two trajectories at initial time t_0, $x(t_0)$ and $y(t_0)$, that are infinitesimally close to each other, i.e., $|x(t_0) - y(t_0)| \to 0$. Then we can say,

$$d(t_0) = |x(t_0) - y(t_0)| \tag{4.10}$$

Consider, these trajectories evolved to time t, $x(t)$ and $y(t)$. Then if,

$$d(t) = |x(t) - y(t)| \tag{4.11}$$

The lyapunov exponent is given by,

$$\lambda = \lim_{t\to\infty} \lim_{d(t_0)\to 0} \left(\frac{1}{t} \ln \frac{d(t)}{d(t_0)} \right) \tag{4.12}$$

For our system, we took $d(t_0)$ to be equal to the distance between two infinitesimally close momentum evolution states for both particle 1 and particle 2. We then evolved the set of two trajectories to get $d(t)$ for both particles 1 and 2. And from these we calculated the lyapunov exponent λ for both particles 1 and 2. This lyapunov exponent was calculated for different times from 300 to 10,000 kicks and plotted. Fig.(4.7)-(4.10) show these lyapunov exponent plots for the 4 cases of α_i and 3 different kicking strengths, $K = 0.1, 1, 10$. We see how the lyapunov exponent for each case of α_i becomes more positive with increasing kicking strength. This clearly shows the transition to chaos for increasing kicking strength.

4.2 Quantum System

We take a look at the quantum linear kicked rotor with a momentum interaction term. The Hamiltonian for this system is,

$$\hat{H} = \hat{H}_0 + \hat{V} \sum_{n=-\infty}^{\infty} \delta(t - n) \tag{4.13}$$

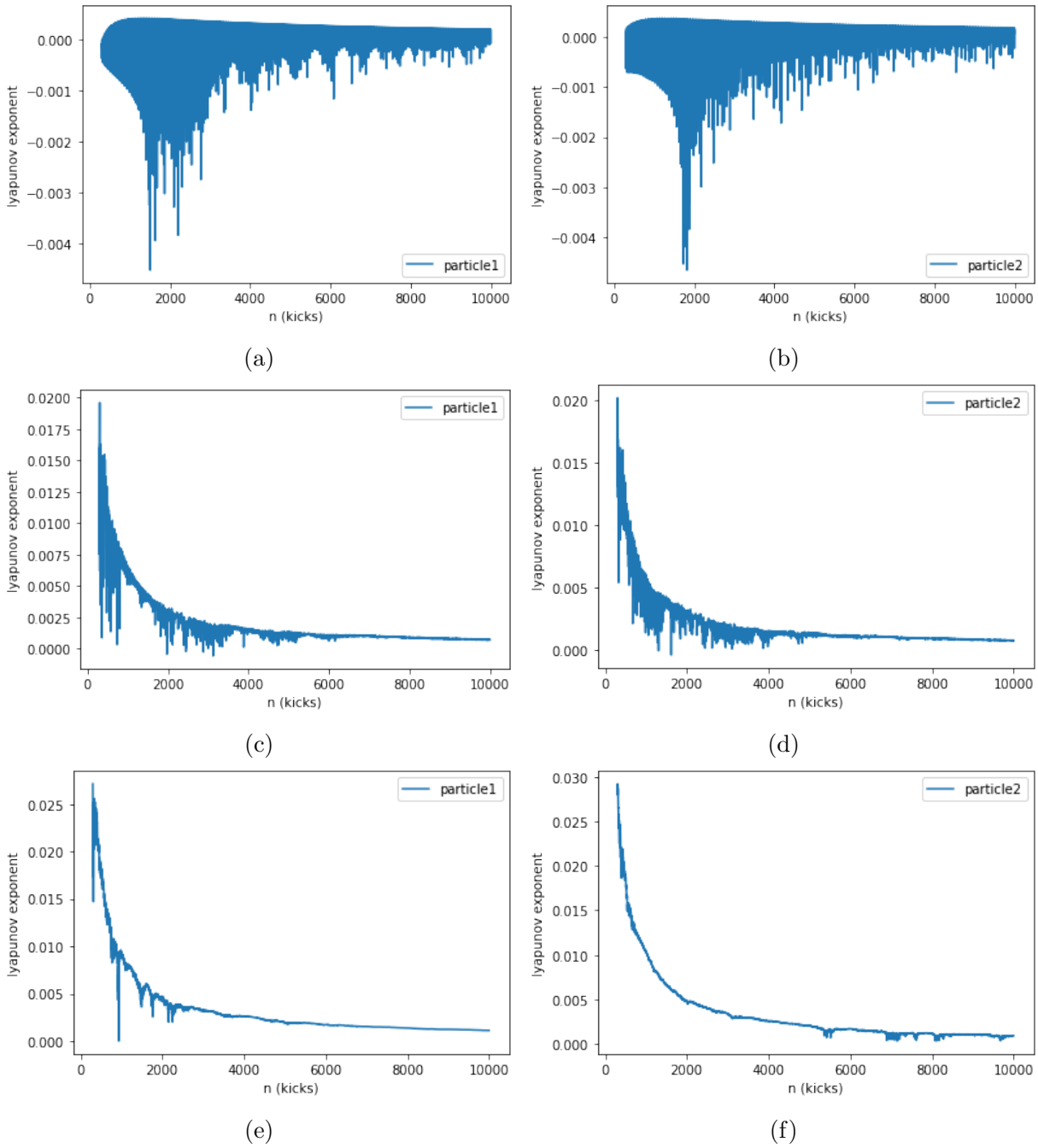

Figure 4.7: Lyapunov exponent for $\alpha_1 = \sqrt{5}$ and $\alpha_2 = \sqrt{3}$. (a),(b) $K = 0.1$; (c),(d) $K = 1$; (e),(f) $K = 10$.

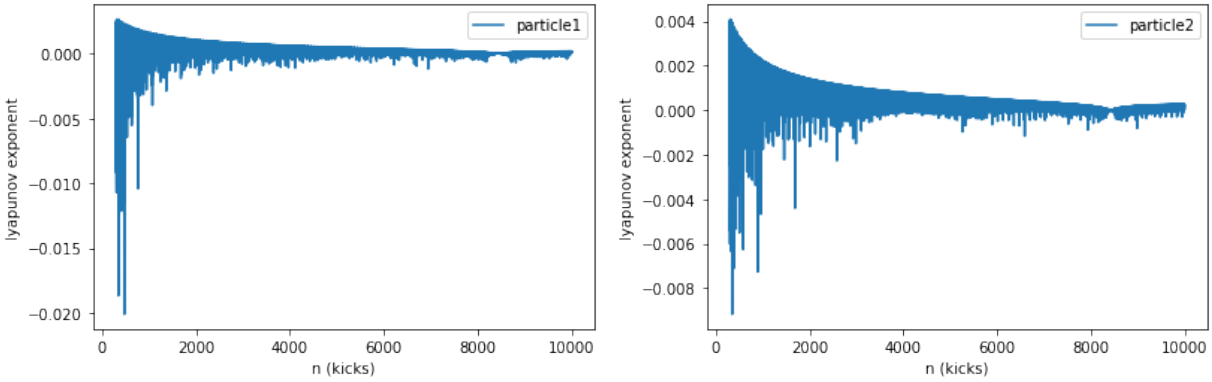

(a)

(b)

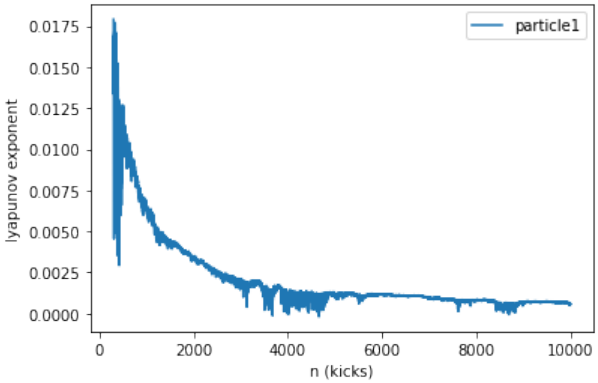

(c)

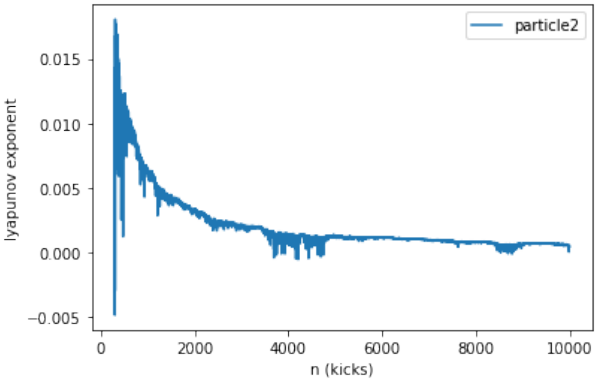

(d)

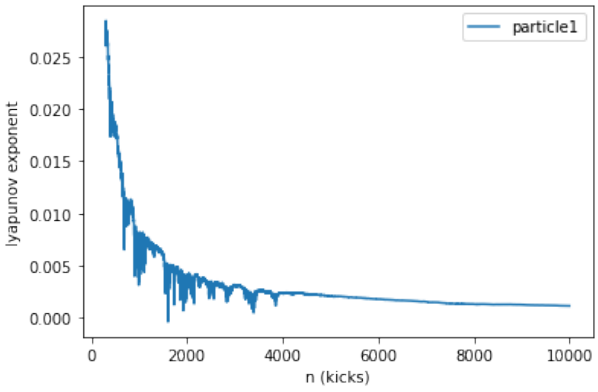

(e)

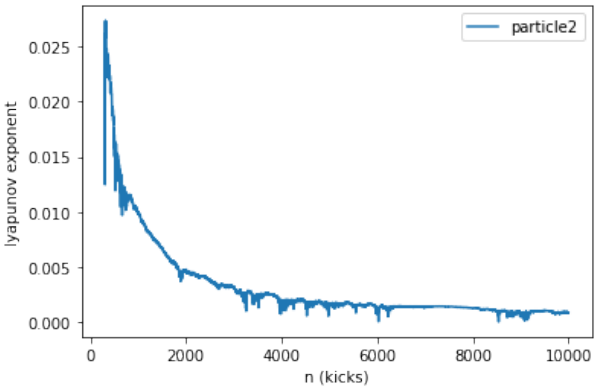

(f)

Figure 4.8: Lyapunov exponent for $\alpha_1 = \sqrt{3}$ and $\alpha_2 = \sqrt{3}$. (a),(b) $K = 0.1$; (c),(d) $K = 1$; (e),(f) $K = 10$.

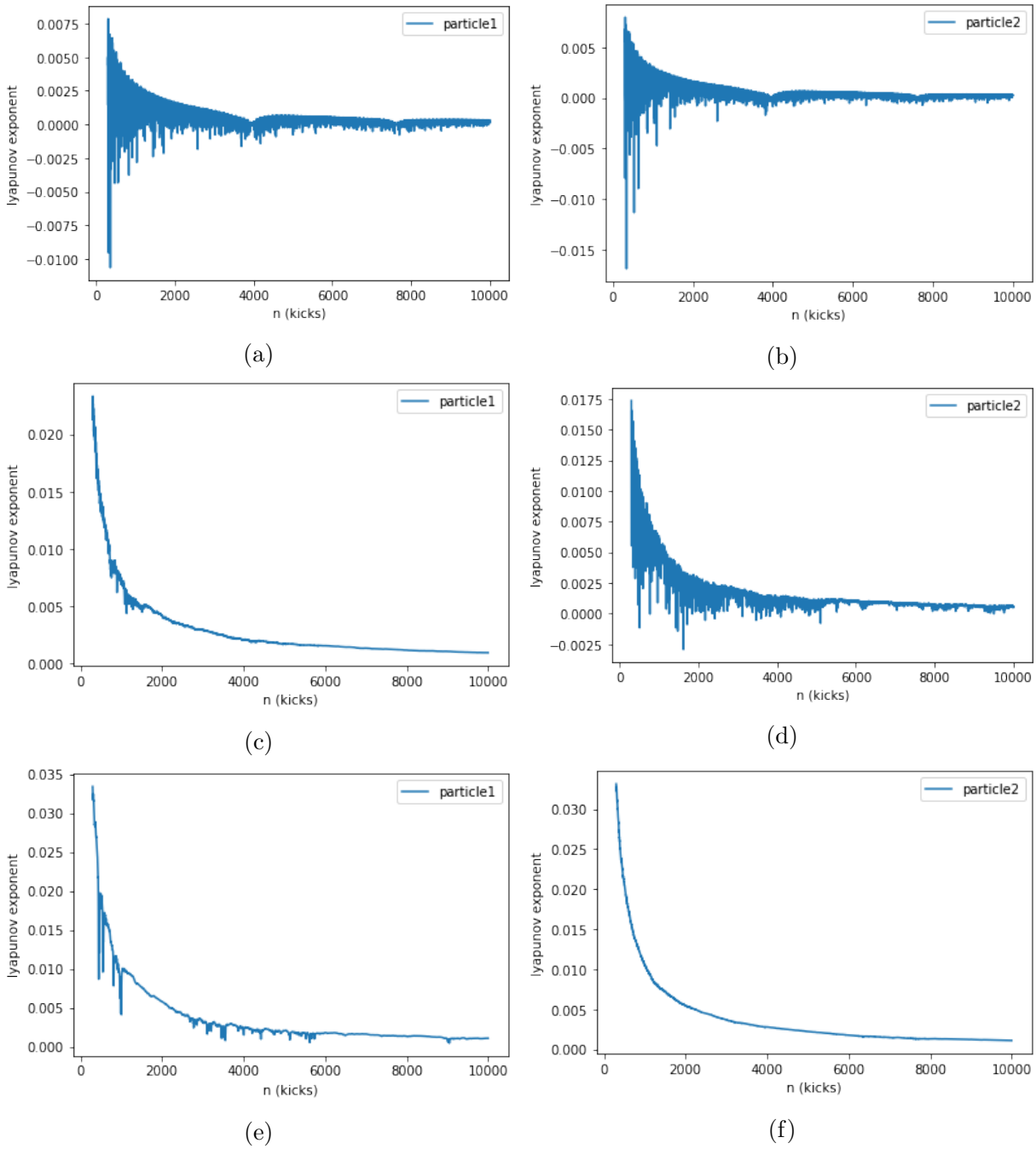

Figure 4.9: Lyapunov exponent for $\alpha_1 = 1$ and $\alpha_2 = \sqrt{3}$. (a),(b) $K = 0.1$; (c),(d) $K = 1$; (e),(f) $K = 10$.

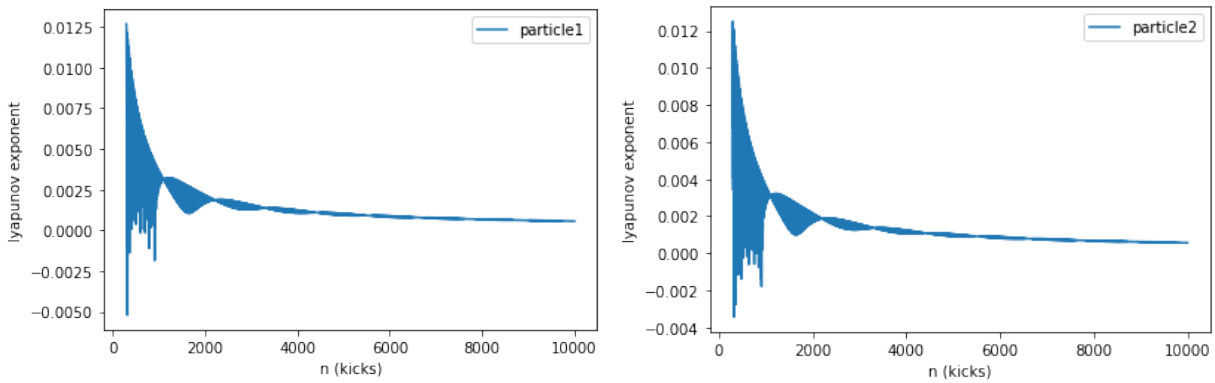

(a)

(b)

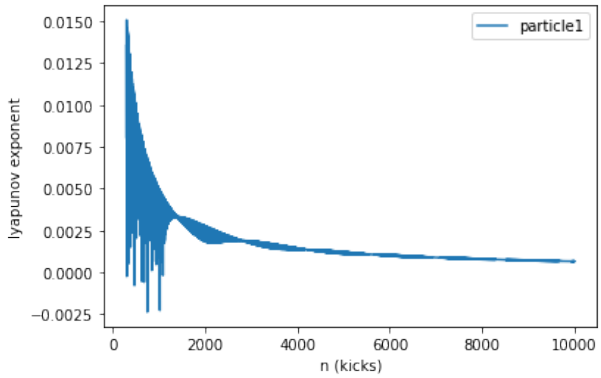

(c)

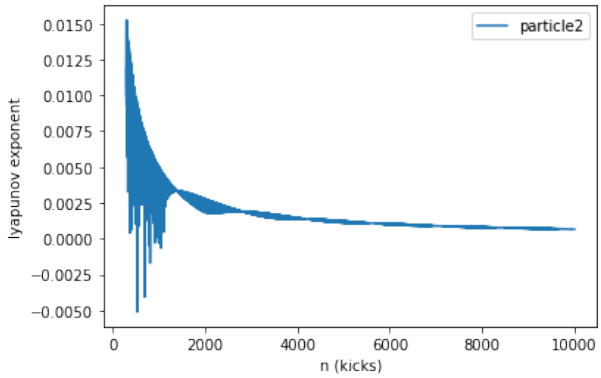

(d)

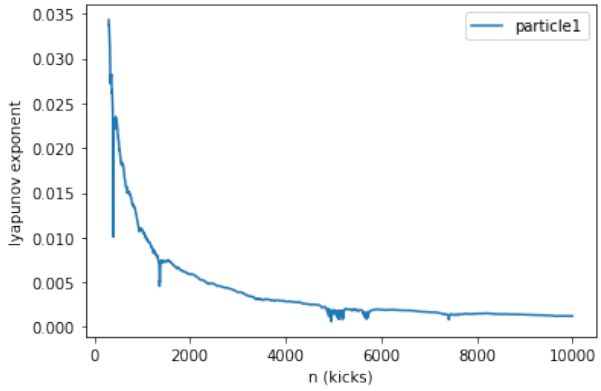

(e)

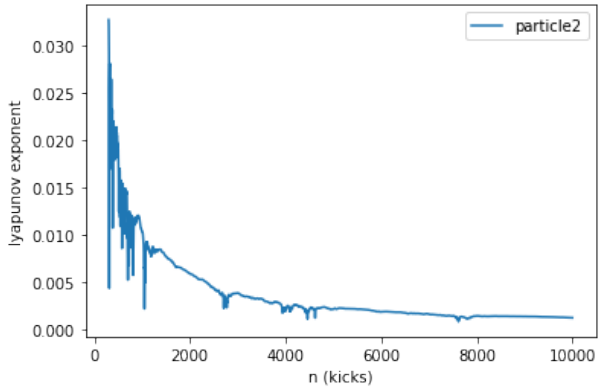

(f)

Figure 4.10: Lyapunov exponent for $\alpha_1 = 1$ and $\alpha_2 = 3$. (a),(b) $K = 0.1$; (c),(d) $K = 1$; (e),(f) $K = 10$.

Where $\hat{H}_0$ is the unperturbed Hamiltonian and is,

$$\hat{H}_0 = 2\pi\alpha_1\hat{p_1} + 2\pi\alpha_2\hat{p_2} + k_p\cos(\hat{p_1} - \hat{p_2}) \tag{4.14}$$

$\hat{V}$ is the kicking potential given by,

$$\hat{V} = K\left[\cos\left(\hat{\theta_1}\right) + \cos\left(\hat{\theta_2}\right)\right] \tag{4.15}$$

and K is the kicking strength.

We look at the evolution of the state of the system. Suppose the state of the system immediately after the nth kick is $|\Psi_n\rangle$. Between nth and $(n+1)$th kick, time evolution is due to the unperturbed Hamiltonian $\hat{H}_0$. This is accomplished with a unitary time evolution operator $\hat{U}_{\hat{H}_0} = e^{-i\hat{H}_0}$. The state of the system after applying this time evolution operator is,

$$\left|\Psi_n^{'}\right\rangle = \hat{U}_{\hat{H}_0}\left|\Psi_n\right\rangle \tag{4.16}$$

Then, the $(n+1)$th kick takes place and the state of the system changes again, this time due to the kicking potential $\hat{V}$. This evolution of state is accomplished by the unitary time evolution operator $\hat{U}_{\hat{V}} = e^{-i\hat{V}}$ acting on the ket $\left|\Psi_n^{'}\right\rangle$ to give the state of the system immediately after the $(n+1)$th kick.

$$|\Psi_{n+1}\rangle = \hat{U}_{\hat{V}}\left|\Psi_n^{'}\right\rangle \tag{4.17}$$

Equations (4.16) and (4.17) can be combined to give,

$$|\Psi_{n+1}\rangle = \hat{U}_{\hat{V}}\hat{U}_{\hat{H}_0}|\Psi_n\rangle \tag{4.18}$$

$\hat{U}_F = \hat{U}_{\hat{V}}\hat{U}_{\hat{H}_0}$ is the Floquet evolution operator of the system.

$$\hat{U}_F = e^{-i\hat{V}}e^{-i\hat{H}_0} \tag{4.19}$$

Given the initial state of the system $|\Psi_0\rangle$, we get the state of the system after Nth kick as,

$$\begin{aligned} |\Psi_N\rangle &= \hat{U}_F^N|\Psi_0\rangle \\ &= (e^{-i\hat{V}}e^{-i\hat{H}_0})^N|\Psi_0\rangle \\ &= e^{-i\hat{V}}e^{-i\hat{H}_0}e^{-i\hat{V}}e^{-i\hat{H}_0}...\,e^{-i\hat{V}}e^{-i\hat{H}_0}|\Psi_0\rangle \end{aligned} \tag{4.20}$$

To calculate the eigenfunctions for our system, we start off in the momentum representation. To calculate the next eigenfunction $|\Psi_1\rangle$,

$$\Psi_1(p) = IFFT(e^{-i\hat{V}}(FFT(e^{-i\hat{H}_0}(\Psi_0(p))))) \tag{4.21}$$

Where FFT and IFFT are fast fourier transform and inverse fast fourier transform respectively. Staring off with $\Psi_0(p)$ in the momentum representation, which we choose as the momentum eigenfunction, we apply the first unitary time evolution operator $e^{-i\hat{H}_0}$ which is diagonal in the momentum variable, hence making calculation in the momentum representation easy. However, $e^{-i\hat{V}}$ is diagonal in the position variable so to apply this unitary time evolution operator and make calculation easy, we apply FFT to go to the position representation. We then apply $e^{-i\hat{V}}$ and finally, to get the new wavefunction $\Psi_1(p)$ in the momentum representation, we apply IFFT. We can then take $\Psi_1(p)$ as our new "initial" wave-function and repeat the process till we get $\Psi_N(p)$, the wave-function immediately after the Nth kick.

Once we have $\Psi_N(p)$ we can then calculate the momentum standard deviation. To do this, we calculate the expectation values of p and p^2 by taking the weighted average over a large number of values. The standard deviation we get will then give us an idea of the momentum dynamics of the system.

We have plotted these momentum standard deviations as a function of time in Fig.(4.11) for the four cases of α_i as before.

4.2.1 Spacing Ratio Distribution

We have calculated the spacing ratio distribution for the system below.

To calculate the spacing ratio distribution for the system, we need to calculate the eigenvalues of the system. Eigenvalues of the system are found by diagonalising the floquet evolution matrix. Therefore the first step is to find the floquet matrix. It is easiest to calculate this matrix in the momentum representation. To do this, we start by calculating the matrix elements of the floquet operator in the momentum basis.

$$\langle p' | \hat{U}_F | p \rangle = \langle p' | e^{-i\hat{V}} e^{-i\hat{H}_0} | p \rangle \tag{4.22}$$

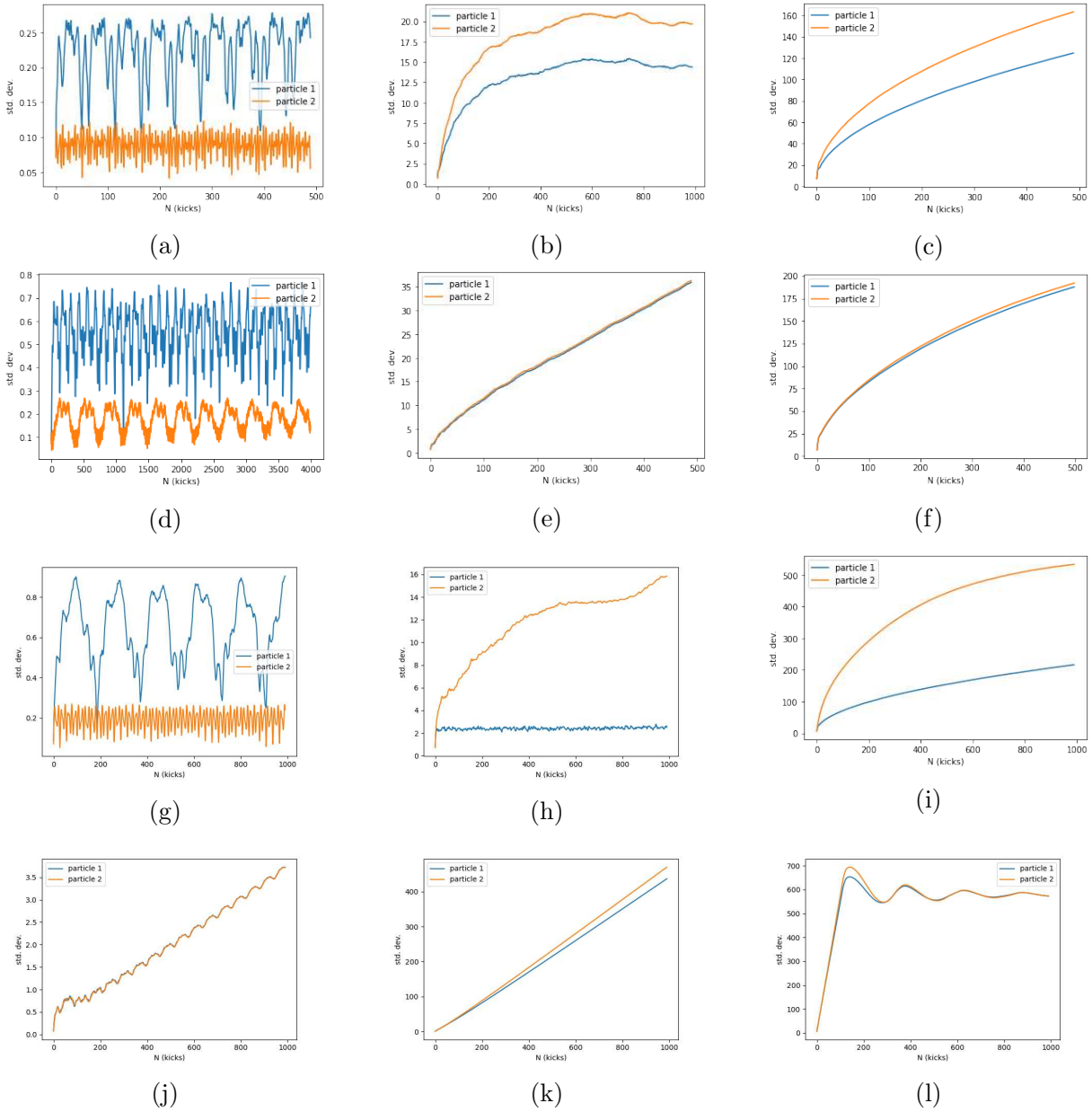

Figure 4.11: Momentum evolution for the different cases of α_i with increasing kicking strength K. (a - c) $\alpha_1 = 1/\sqrt{5}$, $\alpha_2 = 1/\sqrt{3}$; (d - f) $\alpha_1 = 1/\sqrt{88}$, $\alpha_2 = 1/\sqrt{88}$; (g - i) $\alpha_1 = 1/\sqrt{88}$, $\alpha_2 = 1$; (j-l) $\alpha_1 = 2$, $\alpha_2 = 1$. $K = 0.1, 1, 10$ for the first, second and third column of the figure respectively

$e^{-i\hat{H}_0}$ is diagonal in momentum, while $e^{-i\hat{V}}$ is diagonal in position, so we get,

$$\langle p^{'}|\,\hat{U}_F\,|p\rangle = \langle p^{'}|\,e^{-i\hat{V}}\,|p\rangle\,e^{-i\hat{H}_0} \tag{4.23}$$

We expand the first term on the right hand side of this equation by inserting the completeness relation for θ.

$$\begin{aligned}
\langle p^{'}|\,e^{-i\hat{V}}\,|p\rangle &= \int d\theta\,\langle p^{'}|\theta\rangle\,\langle\theta|\,e^{-i\hat{V}}\,|p\rangle \\
&= \int d\theta \frac{e^{-i\vec{p}^{'}\vec{\theta}}}{(\sqrt{2\pi})^2} e^{-i\hat{V}(\vec{\theta})}\,\langle\theta|p\rangle \\
&= \int \frac{d\theta}{(2\pi)^2} e^{i(\vec{p}-\vec{p}^{'})\vec{\theta}} e^{-iK(\cos\vec{\theta}_1+\cos\vec{\theta}_2)} \\
&= \int \frac{d\theta_1}{(2\pi)} e^{i(p_1-p_1^{'})\theta_1} e^{-iK\cos\theta_1} \times \int \frac{d\theta_2}{(2\pi)} e^{i(p_2-p_2^{'})\theta_2} e^{-iK\cos\theta_2} \\
&= (-i)^{p_1-p_1^{'}} J_{p_1-p_1^{'}}(K)(-i)^{p_2-p_2^{'}} J_{p_2-p_2^{'}}(K)
\end{aligned} \tag{4.24}$$

Here, $J_{p_1-p_1^{'}}(K)$ and $J_{p_2-p_2^{'}}(K)$ are Bessel functions.

Therefore, the matrix elements of the floquet operator are,

$$\langle p^{'}|\,\hat{U}_F\,|p\rangle = e^{-ik_p\cos(p_1-p_2)} e^{-i(2\pi\alpha_1 p_1+2\pi\alpha_2 p_2)} (-i)^{(p_1+p_2)-(p_1^{'}+p_2^{'})} J_{p_1-p_1^{'}}(K) J_{p_2-p_2^{'}}(K) \tag{4.25}$$

Now, if $p_1, p_2, p_1^{'}, p_2^{'} \to \infty$, putting the various values of $p_1, p_2, p_1^{'}, p_2^{'}$ into the above equation will give the floquet operator matrix. Then diagonalising this matrix gives its eigenvalues e_i. The eigevalues are then sorted in ascending order such that, $e_1 < e_2 < ....$ The spacing between eigenvalues is found as,

$$s_i = e_{i+1} - e_i \tag{4.26}$$

The spacing ratios are then found as,

$$r_i = \frac{s_{i+1}}{s_i} \tag{4.27}$$

Once the spacing ratios are found, their probability distribution is found and plotted. From the figures Fig.(4.12), the spacing ratios show how the system tends to localisation for increasing values of kicking strength. We see this in the relatively good fit of the numerically calculated distribution with the Poisson distribution as the K values increase. The cases

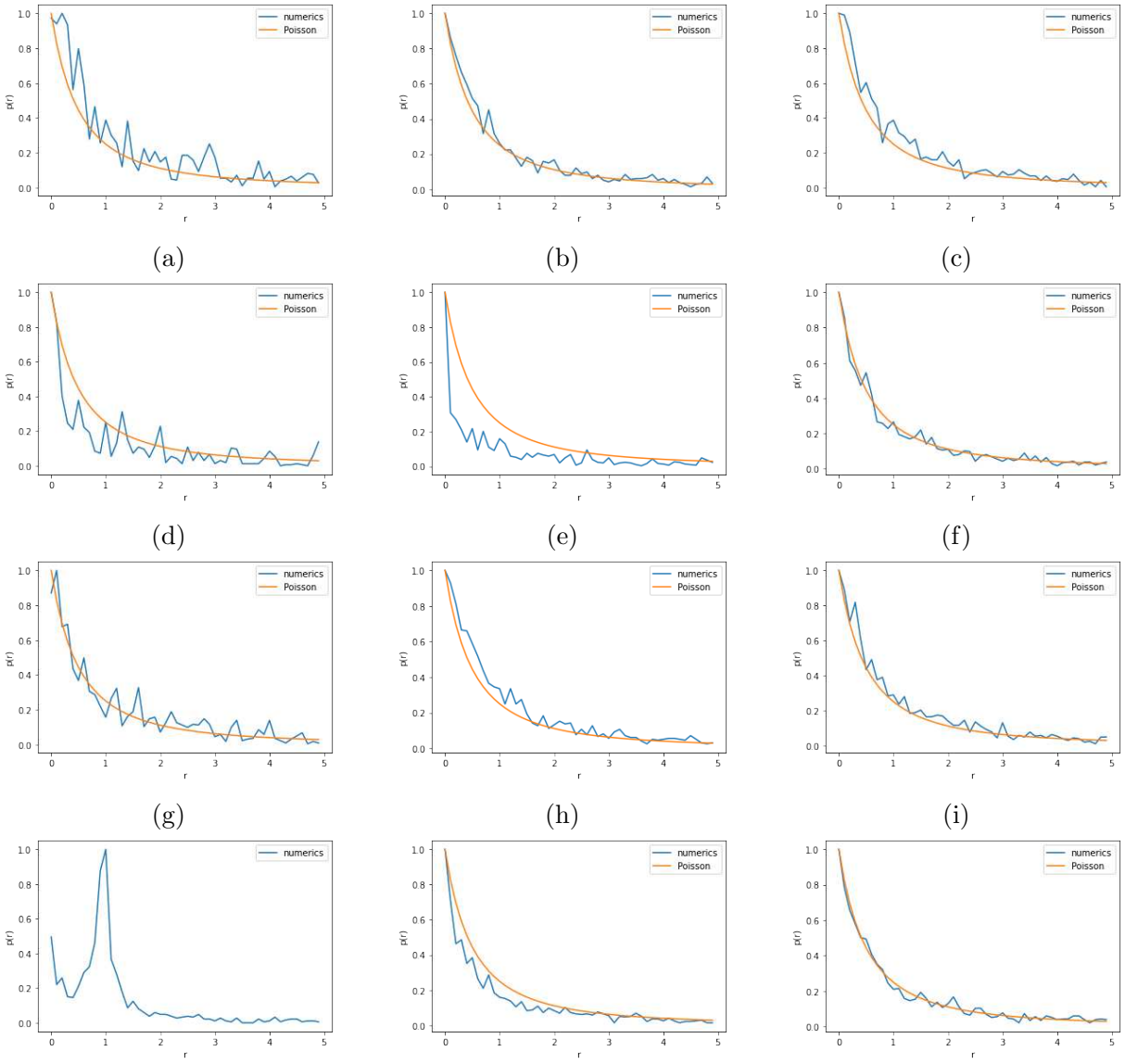

Figure 4.12: Spacing ratio distribution for the different cases of α_i with increasing kicking strength K. (a - c) $\alpha_1 = \sqrt{5}$, $\alpha_2 = \sqrt{3}$; (d - f) $\alpha_1 = \sqrt{3}$, $\alpha_2 = \sqrt{3}$; (g-i) $\alpha_1 = \sqrt{3}$, $\alpha_2 = 1$; (j-l) $\alpha_1 = 1$, $\alpha_2 = 2$. $K = 0.1, 1, 10$ for the first, second and third column of the figure respectively

that show de-localisation show less of a fit to the Poisson distribution. Currently we do not understand the origins of the deviation from the poissonian distribution.

Chapter 5

Conclusion

The many-body localised linear kicked rotor system is interesting in that it shows localisation and delocalisation depending on the values of its parameters. This difference in dynamics has had an interesting effect on the entanglement entropy of the system. For entanglement entropy, calculated for the evolution wavefunction, we have observed that depending on the "level" of delocalisation, we see different kinds of entanglement entropy dynamics. If just one particle in the n-particle system is delocalised in momentum then the entanglement entropy is periodic as opposed to what we expected to see, i.e., logarithmic increase as seen in the other cases of delocalisation in the system when the momentum of more than one particle was delocalised. This dynamics of entropy is in fact similar to what we observed for the case of complete localisation in the dynamics of the system.

We have also calculated the entanglement entropy for the quasi-energy wave-function which remained a constant value depending on parameters, for different eigenvalues of the system. This seems to suggest thermalisation taking place in the system for these wave-functions. The information entropy on the other hand is always a constant, both for evolution as well as quasi-energy wave-function, independent of the parameters of the system.

We have explicitly shown the similarity in the dynamics of the classical system with the quantum system as well as the absence of chaos through Poincare sections for each particle in the system. We then induced chaos in the system by introducing a momentum interaction term in place of the theta interaction term and observed how this changes the dynamics of the system. The transition to chaos with increasing kicking strength was explicitly observed

through Poincare sections, power spectra as well as lyaponov exponents for different values of parameters.

Finally, we looked at the quantum system with the momentum interaction term and saw that localisation and delocalisation are still observed in the system but for different conditions of the parameters as before in the theta interaction case.

Bibliography

[1] Keser A. C., Ganeshan S., Refael G., Galitski V., Dynamical many-body localization in an integrable model, Phys. Rev. B 94, 085120 (2016), DOI: 10.1103/PhysRevB.94.085120

[2] Berry M.V., Incommensurability in an exactly-soluble quantal and classical model for a kicked rotator, Physica 10D, (1984) 369-378, DOI: https://doi.org/10.1016/0167-2789(84)90185-4

[3] Parker S., Bose S., Plenio M. B., Entanglement quantification and purification in continuous variable systems, Phys. Rev. A 61, 032305 (2000), DOI:https://doi.org/10.1103/PhysRevA.61.032305

[4] Atas Y. Y., Bogomolny E., Giraud O., Roux G., Distribution of the Ratio of Consecutive Level Spacings in Random Matrix Ensembles, Phys. Rev. Lett. 110, 084101 (2013), DOI: 10.1103/PhysRevLett.110.084101

[5] Strogatz S. H., Non-Linear Dynamics and Chaos: With Applications to Physics, Biology, Chemistry, and Engineering, Taylor and Francis (2014), 366-369

[6] Dumont R. S., Brumer P., Characteristics of power spectra for regular and chaotic systems, J. Chem. Phys. 88, 1481 (1988), DOI: https://doi.org/10.1063/1.454126

[7] Semmlow J., Signals and Systems for Bioengineers (Second Edition), Academic Press, 2012, 131-165